Asymptotic Performance of Discrete-Valued Vector Reconstruction via Box-Constrained Optimization with Sum of ℓ_1 Regularizers

Ryo Hayakawa, *Member, IEEE*, and Kazunori Hayashi, *Member, IEEE*

***Abstract*—In this paper, we analyze the asymptotic performance of convex optimization-based discrete-valued vector reconstruction from linear measurements. We firstly propose a box-constrained version of the conventional sum of absolute values (SOAV) optimization, which uses a weighted sum of ℓ_1 regularizers as a regularizer for the discrete-valued vector. We then derive the asymptotic symbol error rate (SER) performance of the box-constrained SOAV (Box-SOAV) optimization theoretically by using the convex Gaussian min-max theorem (CGMT). We also derive the asymptotic distribution of the estimate obtained by the Box-SOAV optimization. On the basis of the asymptotic results, we can obtain the optimal parameters of the Box-SOAV optimization in terms of the asymptotic SER. Moreover, we can also optimize the quantizer to obtain the final estimate of the unknown discrete-valued vector. Simulation results show that the empirical SER performance of Box-SOAV and the conventional SOAV is very close to the theoretical result for Box-SOAV when the problem size is sufficiently large. We also show that we can obtain better SER performance by using the proposed asymptotically optimal parameters and quantizers compared to the case with some fixed parameter and a naive quantizer.**

***Index Terms*—Discrete-valued vector reconstruction, convex optimization, convex Gaussian min-max theorem, asymptotic performance**

I. Introduction

RECONSTRUCTION of a discrete-valued vector from its linear measurements often arises in various communications systems, e.g., multiple-input multiple-output (MIMO) signal detection [1], [2], multiuser detection [3], and the decoding of space-time block codes [4]. In some applications such as overloaded MIMO systems [5]–[7] and faster-than-Nyquist (FTN) signaling [8], the number of measurements is less than that of the unknown variables. In such underdetermined problems, simple linear methods, such as linear minimum mean-square-error (LMMSE) method, have poor performance. Although the maximum likelihood (ML) method with the exhaustive search can achieve good performance in terms of the error rate, the computational complexity increases exponentially along with the problem size.

To obtain good performance with reasonable computational complexity, some convex optimization-based methods have been proposed for large-scale discrete-valued vector reconstruction. Box relaxation method [9], [10] considers the ML method under the hypercube including all possible discrete-valued vectors. Regularization-based method and transform-based method [11] apply the idea of compressed sensing [12], [13] to discrete-valued vector reconstruction. Sum of absolute values (SOAV) optimization [14] takes a similar approach and uses a weighted sum of ℓ_1 regularizers as a regularizer for the discrete-valued vector. One of advantages of the SOAV optimization over the other convex optimization-based methods is that it can take the probability distribution of unknown variables into consideration. The SOAV optimization has been applied to various practical problems in wireless communication and control theory [15]–[22].

There are a few theoretical analyses for the convex optimization-based discrete-valued vector reconstruction. For the regularization-based method and the transform-based method, for example, the required number of measurements for the perfect reconstruction has been derived under some assumptions in [11]. As a precise asymptotic analysis, the symbol error rate (SER) performance of the box relaxation method has been analyzed in [23]. The key technique in the analysis is the convex Gaussian min-max theorem (CGMT) [24].

CGMT has been applied to the performance analyses of various optimization problems. The asymptotic normalized-squared-error (NSE) and mean-square-error (MSE) have been analyzed for various regularized estimators [24]–[28]. The asymptotic symbol error rate (SER) of the box relaxation method has been derived for binary phase shift keying (BPSK) signals in [29], and the result has been generalized for pulse amplitude modulation (PAM) in [23]. CGMT has also been used for the analysis of nonlinear measurement model [30]. A similar result has been obtained for MIMO signal detection with low resolution analog-to-digital converters (ADCs), where the receiver has the quantized measurements [31]. Moreover, CGMT can be applied to the case when the measurement matrix is not perfectly known and includes Gaussian distributed errors [32]. In [33], the technique has been used to derive the asymptotically optimal power allocation between the pilots and the data in MIMO BPSK transmission. In [34],

Manuscript received April XX, 20XX; revised September XX, 20XX.
This work was supported in part by the Grants-in-Aid for Scientific Research no. 18K04148 and 18H03765 from the Ministry of Education, Culture, Sports, Science and Technology of Japan, the Grant-in-Aid for JSPS Research Fellow no. 17J07055 from Japan Society for the Promotion of Science, and the R&D contract (FY2017-2020) "Wired-and-Wireless Converged Radio Access Network for Massive IoT Traffic" (JPJ000254) for radio resource enhancement by the Ministry of Internal Affairs and Communications, Japan. This work was partially presented in IEEE ICASSP 2019, Brighton, UK, May 12–17, 2019.

Ryo Hayakawa is with Graduate School of Engineering Science, Osaka University, Osaka 560-8531, Japan (e-mail: rhayakawa@sys.es.osaka-u.ac.jp).
Kazunori Hayashi is with the Center for Innovative Research and Education in Data Science, Kyoto University, Kyoto 606-8315, Japan (e-mail: hayashi.kazunori.4w@kyoto-u.ac.jp).

CGMT-based analysis has been applied to an optimization problem in the complex-valued domain under some assumptions, while above approaches consider optimization problems in the real-valued domain.

In this paper, motivated by the CGMT-based analysis for the box relaxation method [23], we analyze the asymptotic performance of discrete-valued vector reconstruction based on the SOAV optimization. To make the analysis simpler, we firstly modify the conventional SOAV optimization into the box-constrained SOAV (Box-SOAV) optimization by using the boundedness of the unknown vector. The Box-SOAV optimization can be regarded as the combination of the box relaxation method and the SOAV optimization. We then investigate the performance of Box-SOAV by using CGMT [24], [27], which has been used for the performance analyses of several convex optimization problems. We provide the asymptotic SER of Box-SOAV in the large system limit with a fixed measurement ratio, which is defined as the ratio of the number of unknown variables to the number of measurements. The asymptotic SER is characterized by the probability distribution of the unknown vector, the measurement ratio, the parameters of Box-SOAV, and the optimizer of a scalar optimization problem. The result enables us to predict the performance of Box-SOAV in the large-scale discrete-valued vector reconstruction. We also derive the asymptotic distribution of the estimate obtained by the Box-SOAV optimization. By using the asymptotic distribution, we can optimize the quantizer for the hard decision of the unknown discrete-valued vector in terms of the asymptotic SER. Moreover, we propose a procedure to choose the parameter value of the Box-SOAV optimization to minimize the asymptotic SER. Simulation results show that the empirical SER performance of the Box-SOAV optimization and the conventional SOAV optimization agrees well with the theoretical result for Box-SOAV in large-scale problems. From the results, we can also see that the proposed asymptotically optimal parameters and quantizer can achieve better performance compared to the case with some fixed parameter and a naive quantizer.

The additional contributions of this paper against the preliminary conference paper [35] is summarized as follows:

- We provide a detailed proof for the theoretical analysis in this paper, whereas we have given only the sketch of the proof in [35] due to space limitation.
- We further derive the asymptotic distribution of the estimate of the unknown vector obtained by the Box-SOAV optimization.
- On the basis of the asymptotic distribution, we provide the asymptotically optimal quantizer.
- We also propose the parameter selection method that minimizes the asymptotic SER.

The rest of the paper is organized as follows. In Section II, we describe the discrete-valued vector reconstruction problem, some conventional methods, and CGMT. We then provide the main analytical results for the Box-SOAV optimization in Section III. The proof for the main theorem is given in Section IV. Section V gives some simulation results, which demonstrate the validity of the theoretical analysis for Box-SOAV. Finally, Section VI presents some conclusions.

In the rest of the paper, we use the following notations. We denote the transpose by $(\cdot)^{\mathsf{T}}$, the identity matrix by $\boldsymbol{I}$, a vector whose elements are all 1 by $\mathbf{1}$, and a vector whose elements are all 0 by $\mathbf{0}$. For a vector $\boldsymbol{z} = [z_1 \cdots z_N]^{\mathsf{T}} \in \mathbb{R}^N$, the ℓ_1 norm and the ℓ_2 norm are given by $\|\boldsymbol{z}\|_1 = \sum_{n=1}^N |z_n|$ and $\|\boldsymbol{z}\|_2 = \sqrt{\sum_{n=1}^N z_n^2}$, respectively. We denote the number of nonzero elements of $\boldsymbol{z}$ by $\|\boldsymbol{z}\|_0$. For a lower semicontinuous convex function $\zeta : \mathbb{R}^N \to \mathbb{R} \cup \{\infty\}$, we define the Moreau envelope and the proximity operator as $\mathrm{env}_\zeta(\boldsymbol{z}) = \min_{\boldsymbol{u}\in\mathbb{R}^N} \left\{\zeta(\boldsymbol{u}) + \frac{1}{2}\|\boldsymbol{u}-\boldsymbol{z}\|_2^2\right\}$ and $\mathrm{prox}_\zeta(\boldsymbol{z}) = \arg\min_{\boldsymbol{u}\in\mathbb{R}^N} \left\{\zeta(\boldsymbol{u}) + \frac{1}{2}\|\boldsymbol{u}-\boldsymbol{z}\|_2^2\right\}$, respectively. When a sequence of random variables $\{Z_n\}$ $(n = 1, 2, \dots)$ converges in probability to Z, we denote $Z_n \xrightarrow{\mathrm{P}} Z$ as $n \to \infty$ or $\mathrm{plim}_{n\to\infty} Z_n = Z$.

II. Preliminaries

A. Discrete-Valued Vector Reconstruction

In this paper, we consider the reconstruction of an N dimensional discrete-valued vector $\boldsymbol{x} = [x_1 \ \cdots \ x_N]^{\mathsf{T}} \in \mathcal{R}^N \subset \mathbb{R}^N$ from its linear measurements given by

$$\boldsymbol{y} = \boldsymbol{A}\boldsymbol{x} + \boldsymbol{v} \in \mathbb{R}^M. \tag{1}$$

Here, $\mathcal{R} = \{r_1, \dots, r_L\}$ $(r_1 < \cdots < r_L)$ is a finite set of possible values for the elements of the unknown vector. The distribution of the element of $\boldsymbol{x}$ is assumed to be known and is given by $\Pr(x_n = r_\ell) = p_\ell$, where $\sum_{\ell=1}^L p_\ell = 1$. $\boldsymbol{A} \in \mathbb{R}^{M\times N}$ is a known measurement matrix composed of independent and identically distributed (i.i.d.) Gaussian random variables with zero mean and variance $1/N$. $\boldsymbol{v} \in \mathbb{R}^M$ is an additive Gaussian noise vector with mean $\mathbf{0}$ and covariance matrix $\sigma_{\mathrm{v}}^2\boldsymbol{I}$. The noise variance σ_{v}^2 is assumed to be known in this paper.

B. Convex Optimization-Based Approaches

For the discrete-valued vector reconstruction, several convex optimization-based approaches have been proposed. Here, we briefly review some conventional methods.

1) Box Relaxation Method [9], [10]: The box relaxation method is based on the ML method given by

$$\min_{\boldsymbol{s}\in\{r_1,\dots,r_L\}^N} \frac{1}{2}\|\boldsymbol{y}-\boldsymbol{A}\boldsymbol{s}\|_2^2. \tag{2}$$

Although the ML method (2) can achieve good performance, the required computational complexity becomes prohibitive when the problem size is large. To tackle this problem, the box relaxation method uses the box constraint $\boldsymbol{s} \in [r_1, r_L]^N$ instead of the constraint $\boldsymbol{s} \in \{r_1, \dots, r_L\}^N$ in (2) as

$$\min_{\boldsymbol{s}\in[r_1,r_L]^N} \frac{1}{2}\|\boldsymbol{y}-\boldsymbol{A}\boldsymbol{s}\|_2^2 \tag{3}$$

because the unknown vector satisfies $\boldsymbol{x} \in \mathcal{R}^N \subset [r_1, r_L]^N$. Since both of the objective function and the feasible region are convex, the optimization problem can be solved with several convex optimization techniques. The asymptotic SER of the box relaxation method has been derived in [23] by using the CGMT framework.

2) Regularization-Based Method [11]: In [11], the regularization-based method given by

$$\min_{\boldsymbol{s}\in\mathbb{R}^N} \sum_{\ell=1}^{L} \|\boldsymbol{s}-r_\ell\boldsymbol{1}\|_1 \text{ subject to } \boldsymbol{y}=\boldsymbol{A}\boldsymbol{s} \tag{4}$$

has been proposed for the discrete-valued vector reconstruction in the noise-free case. This method uses the regularizer $\sum_{\ell=1}^{L}\|\boldsymbol{s}-r_\ell\boldsymbol{1}\|_1$ for the unknown discrete-valued vector. The idea of the regularizer comes from compressed sensing [12], [13] and the fact that the vector $\boldsymbol{x}-r_\ell\boldsymbol{1}$ has some zero elements. As described in [11], the optimization problem (4) can be solved as linear programming. As for the theoretical analysis, the SER of the regularization-based method has been derived for the binary vector reconstruction. Some methods based on a similar idea have also been proposed for the noisy measurement case [36], [37]. However, these methods cannot utilize the knowledge of the distribution of the unknown vector.

3) SOAV Optimization [14]: The SOAV optimization for the reconstruction of $\boldsymbol{x}$ is given by

$$\min_{\boldsymbol{s}\in\mathbb{R}^N}\left\{\frac{1}{2}\|\boldsymbol{y}-\boldsymbol{A}\boldsymbol{s}\|_2^2+\sum_{\ell=1}^{L} q_\ell\|\boldsymbol{s}-r_\ell\boldsymbol{1}\|_1\right\}, \tag{5}$$

where q_ℓ (≥ 0) is a parameter and set as $q_\ell=p_\ell$ in [14]. Although the SOAV optimization is based on a similar idea as that of the regularization-based method (4), it includes the parameter q_ℓ in the objective function. By tuning these parameters, we can take the probability $p_1,\ldots,p_L$ into account. Since the objective function of the SOAV optimization (5) is convex, we can obtain a sequence converging to the optimal solution by several convex optimization algorithms such as proximal splitting methods [38]. For example, an algorithm based on Beck-Teboulle proximal gradient algorithm [39] has been proposed in [17], whereas Douglas-Rachford algorithm [40], [41] has been used in [19], [21]. Although some theoretical results about the SOAV optimization have been derived in [17], [19] by using restricted isometry property (RIP) [42], the precise SER has not been obtained in the literature.

C. CGMT

CGMT is a theorem that associates the primary optimization (PO) problem with the auxiliary optimization (AO) problem given by

$$\text{(PO): } \Phi(\boldsymbol{G})=\min_{\boldsymbol{w}\in\mathcal{S}_{\rm w}}\max_{\boldsymbol{u}\in\mathcal{S}_{\rm u}}\left\{\boldsymbol{u}^{\mathsf{T}}\boldsymbol{G}\boldsymbol{w}+\rho(\boldsymbol{w},\boldsymbol{u})\right\}, \tag{6}$$

$$\text{(AO): } \phi(\boldsymbol{g},\boldsymbol{h})=\min_{\boldsymbol{w}\in\mathcal{S}_{\rm w}}\max_{\boldsymbol{u}\in\mathcal{S}_{\rm u}}\left\{\|\boldsymbol{w}\|_2\boldsymbol{g}^{\mathsf{T}}\boldsymbol{u}-\|\boldsymbol{u}\|_2\boldsymbol{h}^{\mathsf{T}}\boldsymbol{w}+\rho(\boldsymbol{w},\boldsymbol{u})\right\}, \tag{7}$$

respectively, where $\boldsymbol{G}\in\mathbb{R}^{M\times N}$, $\boldsymbol{g}\in\mathbb{R}^M$, $\boldsymbol{h}\in\mathbb{R}^N$, $\mathcal{S}_{\rm w}\subset\mathbb{R}^N$, $\mathcal{S}_{\rm u}\subset\mathbb{R}^M$, and $\rho(\cdot,\cdot):\mathbb{R}^N\times\mathbb{R}^M\to\mathbb{R}$. We assume that $\mathcal{S}_{\rm w}$ and $\mathcal{S}_{\rm u}$ are closed compact sets, and $\rho(\cdot,\cdot)$ is a continuous convex-concave function on $\mathcal{S}_{\rm w}\times\mathcal{S}_{\rm u}$. The elements of $\boldsymbol{G}$, $\boldsymbol{g}$, and $\boldsymbol{h}$ are i.i.d. standard Gaussian random variables. The following theorem relates the optimizer $\hat{\boldsymbol{w}}_\Phi(\boldsymbol{G})$ of (PO) with the optimal value of (AO) in the limit of $M,N\to\infty$ with a fixed ratio $\Delta=M/N$, which we simply denote $N\to\infty$ in this paper.

Theorem II.1 (CGMT [23])**.** Let $\mathcal{S}$ be an open set in $\mathcal{S}_{\rm w}$ and $\mathcal{S}^{\rm c}=\mathcal{S}_{\rm w}\setminus\mathcal{S}$. Also, let $\phi_{\mathcal{S}^{\rm c}}(\boldsymbol{g},\boldsymbol{h})$ be the optimal value of (AO) with the constraint $\boldsymbol{w}\in\mathcal{S}^{\rm c}$. If there are constants $\eta>0$ and $\bar{\phi}$ satisfying (i) $\phi(\boldsymbol{g},\boldsymbol{h})\leq\bar{\phi}+\eta$ and (ii) $\phi_{\mathcal{S}^{\rm c}}(\boldsymbol{g},\boldsymbol{h})\geq\bar{\phi}+2\eta$ with probability approaching 1, then we have $\lim_{N\to\infty}\Pr\left(\hat{\boldsymbol{w}}_\Phi(\boldsymbol{G})\in\mathcal{S}\right)=1$.

III. Main Results

In this section, we provide the main results of this paper. In Section III-A, we modify the conventional SOAV optimization into the Box-SOAV optimization to make the analysis simpler. In Section III-B, we derive the asymptotic SER of the estimate obtained by the Box-SOAV optimization. We then characterize the distribution of the estimate in Section III-C. By using the results, we also derive the asymptotically optimal quantizer for the estimate in Section III-D. Finally, we propose a parameter selection method for the Box-SOAV optimization in Section III-E.

A. Box-SOAV Optimization

To make the analysis simpler (For details of the analysis, see Section IV-A), we have newly considered the Box-SOAV optimization given by

$$\hat{\boldsymbol{x}}=\arg\min_{\boldsymbol{s}\in[r_1,r_L]^N}\left\{\frac{1}{2}\|\boldsymbol{y}-\boldsymbol{A}\boldsymbol{s}\|_2^2+\sum_{\ell=1}^{L}q_\ell\|\boldsymbol{s}-r_\ell\boldsymbol{1}\|_1\right\} \tag{8}$$

$$=\arg\min_{\boldsymbol{s}\in\mathbb{R}^N}\left\{\frac{1}{2}\|\boldsymbol{y}-\boldsymbol{A}\boldsymbol{s}\|_2^2+\sum_{\ell=1}^{L}q_\ell\|\boldsymbol{s}-r_\ell\boldsymbol{1}\|_1+\mathcal{I}(\boldsymbol{s})\right\}, \tag{9}$$

where the function $\mathcal{I}(\cdot)$ denotes the indicator function given by

$$\mathcal{I}(\boldsymbol{s})=\begin{cases}0 & (\boldsymbol{s}\in[r_1,r_L]^N)\\ \infty & (\boldsymbol{s}\notin[r_1,r_L]^N)\end{cases}. \tag{10}$$

This modification is reasonable because $\boldsymbol{x}\in[r_1,r_L]^N$ and it does not change the value of the objective function for $\boldsymbol{s}\in[r_1,r_L]^N$. Let $f(\boldsymbol{s})=\sum_{\ell=1}^{L}q_\ell\|\boldsymbol{s}-r_\ell\boldsymbol{1}\|_1+\mathcal{I}(\boldsymbol{s})$, where $f(\cdot)$ is an element-wise function and we use the same notation $f(\cdot)$ for the corresponding scalar function hereafter. By modifying the result in [17], the proximity operator $\mathrm{prox}_{\gamma f}(z)$ ($\gamma\geq 0$) can be obtained as

$$\mathrm{prox}_{\gamma f}(z)=\begin{cases}r_1 & (z<r_1+\gamma Q_2)\\ \vdots & \vdots\\ z-\gamma Q_k & (r_{k-1}+\gamma Q_k\leq z<r_k+\gamma Q_k)\\ r_k & (r_k+\gamma Q_k\leq z<r_k+\gamma Q_{k+1})\\ \vdots & \vdots\\ r_L & (r_L+\gamma Q_L\leq z)\end{cases}, \tag{11}$$

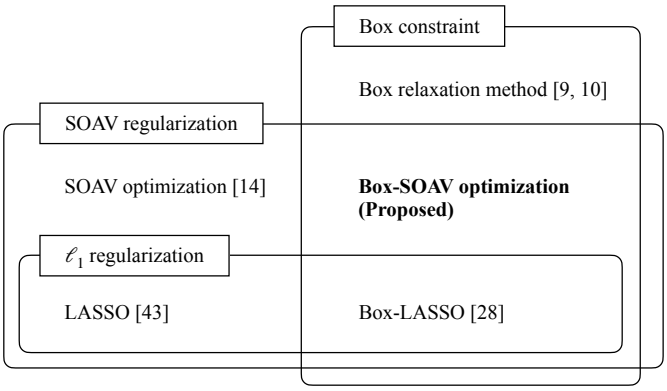

Fig. 1: Relationship to conventional methods

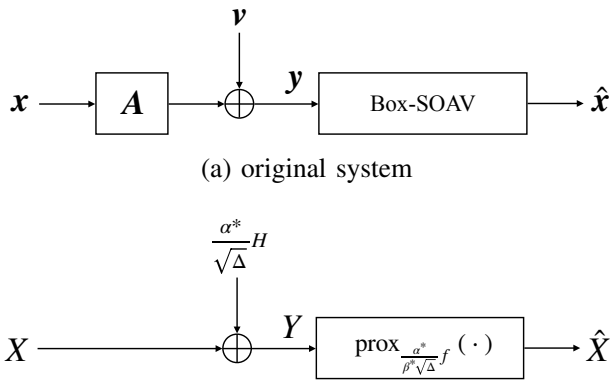

(a) original system

(b) decoupled scalar system

Fig. 2: Comparison between the original reconstruction process and its decoupled version in the asymptotic regime

where

$$Q_k = \left(\sum_{\ell=1}^{k-1} q_\ell\right) - \left(\sum_{\ell'=k}^{L} q_{\ell'}\right) \quad (k = 2, \ldots, L). \tag{12}$$

By using some proximal splitting algorithm [38] with the proximity operator in (11), we can obtain a sequence converging to the solution of the Box-SOAV optimization (9).

It should be noted that the Box-SOAV optimization in (9) is the combination of the box relaxation method in (3) and the SOAV optimization in (5). Figure 1 shows the relationship between the Box-SOAV optimization and several conventional methods. Unlike the Box relaxation method, the Box-SOAV optimization utilizes both the box constraint and the SOAV regularization. Hence, the Box-SOAV optimization can utilize the knowledge of the distribution $p_1, \ldots, p_L$ and can achieve better performance than the box relaxation method when the distribution is not uniform. It should also be noted that the ℓ_1 regularization $\|\boldsymbol{s}\|_1$ in absolute shrinkage and selection operator (LASSO) [43] is a special case of the SOAV regularization $\sum_{\ell=1}^{L} q_\ell \|\boldsymbol{s} - r_\ell \boldsymbol{1}\|_1$. As the combination of the box constraint and the ℓ_1 regularization, the box constrained-LASSO (Box-LASSO) given by

$$\min_{\boldsymbol{s}\in[c_{\mathrm{l}}, c_{\mathrm{u}}]^N} \left\{ \frac{1}{2} \|\boldsymbol{y} - \boldsymbol{A}\boldsymbol{s}\|_2^2 + \lambda \|\boldsymbol{s}\|_1 \right\} \tag{13}$$

has been discussed in the literature [28], where λ (> 0) is the regularization parameter. The Box-SOAV optimization can be regarded as an extension of Box-LASSO for general discrete distribution. In fact, Box-SOAV becomes equivalent to Box-LASSO in some cases (For example, see Example III.2).

B. Asymptotic SER of Box-SOAV

To provide the asymptotic SER of Box-SOAV, we firstly show the following theorem.

Theorem III.1. The measurement matrix $\boldsymbol{A} \in \mathbb{R}^{M\times N}$ is assumed to be composed of i.i.d. Gaussian random variables with zero mean and variance $1/N$. The distribution of the noise vector $\boldsymbol{v} \in \mathbb{R}^M$ is also assumed to be Gaussian with mean $\boldsymbol{0}$ and covariance matrix $\sigma_{\mathrm{v}}^2 \boldsymbol{I}$. We also assume that the optimization problem $\max_{\beta>0} \min_{\alpha>0} F(\alpha, \beta)$ has a unique optimizer (α^*, β^*), where

$$F(\alpha,\beta) = \frac{\alpha\beta\sqrt{\Delta}}{2} + \frac{\sigma_{\mathrm{v}}^2\beta\sqrt{\Delta}}{2\alpha} - \frac{1}{2}\beta^2 - \frac{\alpha\beta}{2\sqrt{\Delta}} + \frac{\beta\sqrt{\Delta}}{\alpha}\mathrm{E}\left[\mathrm{env}_{\frac{\alpha}{\beta\sqrt{\Delta}}f}\left(X + \frac{\alpha}{\sqrt{\Delta}}H\right)\right]. \tag{14}$$

Here, X is the random variable with the same distribution as the unknown variables, i.e., $\Pr(X = r_\ell) = p_\ell$. H is the standard Gaussian random variable independent of X. We further define

$$\mathcal{L} = \{\psi(\cdot,\cdot) : [r_1 - r_L, r_L - r_1] \times \mathcal{R} \to \mathbb{R} \mid \psi(\cdot, r_\ell) \text{ is Lipschitz continuous for any } r_\ell \in \mathcal{R}\}. \tag{15}$$

For any function $\psi(\cdot,\cdot) \in \mathcal{L}$, we have

$$\operatorname*{plim}_{N\to\infty} \frac{1}{N}\sum_{n=1}^{N} \psi\left(\hat{x}_n - x_n, x_n\right) = \mathrm{E}\left[\psi\left(\hat{X} - X, X\right)\right], \tag{16}$$

where $\hat{x}_n$ denotes the nth element of $\hat{\boldsymbol{x}}$ in (9) and

$$\hat{X} = \mathrm{prox}_{\frac{\alpha^*}{\beta^*\sqrt{\Delta}}f}\left(X + \frac{\alpha^*}{\sqrt{\Delta}}H\right). \tag{17}$$

Proof: See Section IV. ■

Theorem III.1 gives us intuitive insights for the discrete-valued vector reconstruction with the Box-SOAV optimization. We can see from (16) that the random variable $\hat{X}$ has the probabilistic property of the estimate $\hat{\boldsymbol{x}}$ (For precise characterization of $\hat{X}$, see Theorem III.2 in Section III-C). Hence, (17) can be regarded as the 'decoupled' scalar system of the original system as shown in Fig. 2, where $Y = X + \frac{\alpha^*}{\sqrt{\Delta}}H$. The unknown vector $\boldsymbol{x}$ is mixed by the measurement matrix $\boldsymbol{A}$ in the original system (Fig. 2(a)), whereas the unknown variable X goes through only the additive Gaussian white noise (AWGN) channel in the decoupled scalar system (Fig. 2(b)). Note that the noise variance $(\alpha^*)^2/\Delta$ is related to the asymptotic MSE

and $\sigma_{\rm v}^2$ in the reconstruction (See Remark IV.1). Moreover, The proximity operator

$$\mathrm{prox}_{\frac{\alpha^*}{\beta^*\sqrt{\Delta}}f}(Y) = \arg\min_{s\in\mathbb{R}} \left\{ \frac{1}{2}(Y-s)^2 + \frac{\alpha^*}{\beta^*\sqrt{\Delta}} f(s) \right\} \tag{18}$$

has the 'decoupled' form of the original Box-SOAV optimization in (9), which can be rewritten as

$$\hat{\boldsymbol{x}} = \arg\min_{\boldsymbol{s}\in\mathbb{R}^N} \left\{ \frac{1}{2}\left\|\boldsymbol{y}-\boldsymbol{A}\boldsymbol{s}\right\|_2^2 + f(\boldsymbol{s}) \right\}, \tag{19}$$

up to the coefficient $\frac{\alpha^*}{\beta^*\sqrt{\Delta}}$. In the asymptotic regime with the large system limit, the statistical property of the reconstruction with the Box-SOAV optimization is characterized by the scalar system given by (17). Such a decoupling principle has also been known for approximate message passing (AMP) algorithm and related methods [44]–[46].

The SER of Box-SOAV is given by $\frac{1}{N}\left\|\mathcal{Q}(\hat{\boldsymbol{x}})-\boldsymbol{x}\right\|_0$, where the element-wise quantizer $\mathcal{Q}(\cdot)$ maps each element of the vector to a value in $\mathcal{R}$. The asymptotic SER of Box-SOAV is given by the following corollary of Theorem III.1.

Corollary III.1. Under the assumptions in Theorem III.1, the asymptotic SER of Box-SOAV is given by

$$\begin{aligned}&\operatorname*{plim}_{N\to\infty}\frac{1}{N}\left\|\mathcal{Q}(\hat{\boldsymbol{x}})-\boldsymbol{x}\right\|_0\\ &= 1-\sum_{\ell=1}^{L} p_\ell \Pr\left(\mathcal{Q}(\hat{X}) = r_\ell \mid X = r_\ell\right).\end{aligned} \tag{20}$$

Proof: See Appendix A. ∎

The function $F(\alpha,\beta)$ in (14) and the asymptotic SER in (20) can be calculated by using the probability density function $p_H(z) = \frac{1}{\sqrt{2\pi}}\exp(-z^2/2)$ and the cumulative distribution function (CDF) $P_H(z) = \int_{-\infty}^{z} p_H(z')dz'$ of the standard Gaussian distribution. For example, when we use the quantizer $\mathcal{Q}_{\rm NV}(\cdot)$ that maps the input to the nearest value in $\mathcal{R}$, i.e.,

$$\mathcal{Q}_{\rm NV}(\hat{x}) = \begin{cases} r_1 & \left(\hat{x} < \dfrac{r_1+r_2}{2}\right) \\ \vdots & \vdots \\ r_\ell & \left(\dfrac{r_{\ell-1}+r_\ell}{2} \le \hat{x} < \dfrac{r_\ell+r_{\ell+1}}{2}\right) \\ \vdots & \vdots \\ r_L & \left(\dfrac{r_{L-1}+r_L}{2} \le \hat{x}\right) \end{cases}, \tag{21}$$

the asymptotic SER in (20) can be written as

$$\begin{aligned}\mathrm{SER}_{\rm NV} = 1-\sum_{\ell=1}^{L} p_\ell \Bigg\{ & P_H\left(\frac{\sqrt{\Delta}}{2\alpha^*}(r_{\ell+1}-r_\ell)+\frac{Q_{\ell+1}}{\beta^*}\right) \\ & - P_H\left(\frac{\sqrt{\Delta}}{2\alpha^*}(r_{\ell-1}-r_\ell)+\frac{Q_\ell}{\beta^*}\right)\Bigg\},\end{aligned} \tag{22}$$

where Q_ℓ is defined in (12) for $\ell = 2,\ldots,L$ and we further define $Q_1 = -\infty$, $Q_{L+1} = \infty$, $r_0 = -\infty$, and $r_{L+1} = \infty$ for convenience.

C. Asymptotic Distribution of Estimates by Box-SOAV

Corollary III.1 implies that the asymptotic distribution of the estimate $\hat{x}_n$ is characterized by the random variable $\hat{X}$ in (17). In fact, we can obtain the following convergence result from Theorem III.1.

Theorem III.2. Let $\mu_{\hat{\boldsymbol{x}}}$ be the empirical distribution corresponding to the CDF given by $P_{\hat{\boldsymbol{x}}}(\hat{x}) = \frac{1}{N}\sum_{n=1}^{N}\mathbb{I}(\hat{x}_n \le \hat{x})$, where $\mathbb{I}(\hat{x}_n \le \hat{x}) = 1$ if $\hat{x}_n \le \hat{x}$ and otherwise $\mathbb{I}(\hat{x}_n \le \hat{x}) = 0$. Moreover, let $\mu_{\hat{X}}$ be the distribution of the random variable $\hat{X}$. The empirical distribution $\mu_{\hat{\boldsymbol{x}}}$ converges weakly in probability to $\mu_{\hat{X}}$, i.e., $\int g\, d\mu_{\hat{\boldsymbol{x}}} \xrightarrow{\rm P} \int g\, d\mu_{\hat{X}}$ holds as $N\to\infty$ for every continuous compactly supported function $g(\cdot):[r_1,r_L]\to\mathbb{R}$.

Proof: See Appendix B. ∎

From Theorem III.2, we can evaluate the asymptotic distribution of the estimate obtained by Box-SOAV. The CDF of $\hat{X}$ is given by

$$P_{\hat{X}}(\hat{x}) = \Pr\left(\hat{X}\le\hat{x}\right) \tag{23}$$

$$= \sum_{\ell=1}^{L} p_\ell \Pr\left(\hat{X}\le\hat{x} \mid X = r_\ell\right) \tag{24}$$

$$= \sum_{\ell=1}^{L} p_\ell \Pr\left(\mathrm{prox}_{\frac{\alpha^*}{\beta^*\sqrt{\Delta}}f}\left(r_\ell+\frac{\alpha^*}{\sqrt{\Delta}}H\right)\le\hat{x}\right) \tag{25}$$

$$= \sum_{\ell=1}^{L} p_\ell P_H\left(\frac{\sqrt{\Delta}}{\alpha^*}\left\{\mathrm{prox}^{-1}_{\frac{\alpha^*}{\beta^*\sqrt{\Delta}}f}(\hat{x}) - r_\ell\right\}\right) \tag{26}$$

for $\hat{x}\in[r_1,r_L]\setminus\mathcal{R}$, where $\mathrm{prox}^{-1}_{\gamma f}(\cdot):[r_1,r_L]\setminus\mathcal{R}\to\mathbb{R}$ is given by

$$\mathrm{prox}^{-1}_{\gamma f}(\hat{x}) = \begin{cases} \hat{x}+\gamma Q_2 & (r_1<\hat{x}<r_2) \\ \vdots & \vdots \\ \hat{x}+\gamma Q_{\ell+1} & (r_\ell<\hat{x}<r_{\ell+1}) \\ \vdots & \vdots \\ \hat{x}+\gamma Q_L & (r_{L-1}<\hat{x}<r_L) \end{cases} \tag{27}$$

from (11). The CDF in (26) is not continuous at $\hat{x}\in\mathcal{R}$ because the random variable $\hat{X}$ has a probability mass at $\hat{x}\in\mathcal{R}$. In fact, the conditional probability mass at $\hat{X} = r_\ell$ can be written as

$$\Pr\left(\hat{X} = r_\ell \mid X = r_k\right)$$

$$= \Pr\left(\mathrm{prox}_{\frac{\alpha^*}{\beta^*\sqrt{\Delta}}f}\left(r_k+\frac{\alpha^*}{\sqrt{\Delta}}H\right) = r_\ell\right) \tag{28}$$

$$= P_H\left(\frac{\sqrt{\Delta}}{\alpha^*}(r_\ell-r_k)+\frac{Q_{\ell+1}}{\beta^*}\right) - P_H\left(\frac{\sqrt{\Delta}}{\alpha^*}(r_\ell-r_k)+\frac{Q_\ell}{\beta^*}\right), \tag{29}$$

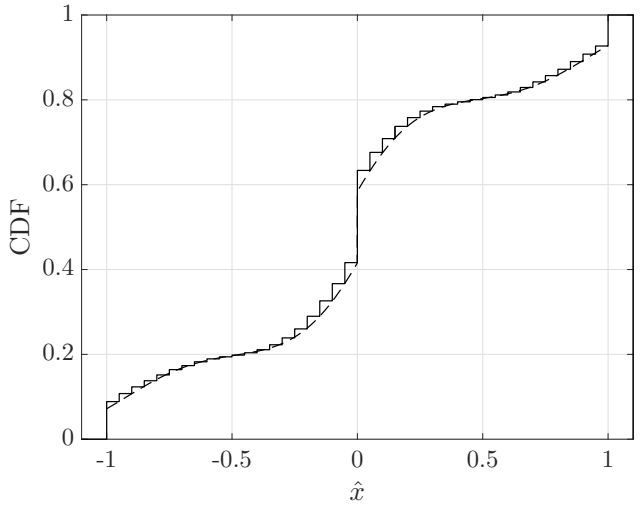

Fig. 3: The empirical histogram of the CDF (solid line) and the asymptotic distribution (dashed line) of the estimates by Box-SOAV ($N = 1000$, $M = 750$, $\Delta = 0.75$, $(p_1, p_2, p_3) = (0.2, 0.6, 0.2)$, $(r_1, r_2, r_3) = (-1, 0, 1)$, $(q_1, q_2, q_3) = (1, 0.005, 1)$, SNR $= 20$ dB)

whereas for $\hat{x} \notin \mathcal{R}$ the conditional density of $\hat{X}$ on the event $X = r_k$ is given by

$$p_{\hat{X}|X=r_k}(\hat{x}) = \frac{\sqrt{\Delta}}{\alpha^*} p_H\left(\frac{\sqrt{\Delta}}{\alpha^*}\left\{\mathrm{prox}^{-1}_{\frac{\alpha^*}{\beta^*\sqrt{\Delta}}f}(\hat{x}) - r_k\right\}\right). \tag{30}$$

Hence, the asymptotic density $p_{\hat{X}}(\hat{x})$ of $\hat{X}$ can be written as

$$p_{\hat{X}}(\hat{x}) = \begin{cases} \sum_{k=1}^{L} p_k \Pr\left(\hat{X} = r_\ell \mid X = r_k\right) \delta_{r_\ell}(\hat{x}) & (\hat{x} = r_\ell) \\ \sum_{k=1}^{L} p_k p_{\hat{X}|X=r_k}(\hat{x}) & (\hat{x} \notin \mathcal{R}) \end{cases}, \tag{31}$$

where $\delta_{r_\ell}(\cdot)$ denotes the Dirac measure at r_ℓ.

In Fig. 3, we show the empirical histogram of the CDF of the estimates by Box-SOAV. In the simulation, we set $N = 1000$, $M = 750$, $\Delta = 0.75$, $(p_1, p_2, p_3) = (0.2, 0.6, 0.2)$, $(r_1, r_2, r_3) = (-1, 0, 1)$, and $(q_1, q_2, q_3) = (1, 0.005, 1)$. The signal-to-noise ratio (SNR) defined as $\sum_{\ell=1}^{L} p_\ell r_\ell^2 / \sigma_v^2$ is 20 dB. The empirical result is averaged over 20 independent realizations of the measurement matrix $\boldsymbol{A}$ and the unknown vector $\boldsymbol{x}$. To solve the Box-SOAV optimization, we use the Douglas-Rachford algorithm [38], [40]. For comparison, the figure also shows the asymptotic distribution in (26). We can see that the asymptotic distribution obtained from Theorem III.2 agrees well with the empirical histogram of the CDF.

D. Asymptotically Optimal Quantizer

By using the asymptotic density in the previous subsection, we can design the quantizer $\mathcal{Q}(\cdot)$ to obtain the asymptotically optimal SER. Although $\mathcal{Q}_{\mathrm{NV}}(\cdot)$ in (21) is commonly used as the quantizer, it is not optimal in terms of the asymptotic SER in (20) in general. We here present the desired quantizer minimizing the asymptotic SER as the asymptotically optimal quantizer $\mathcal{Q}_{\mathrm{AO}}(\hat{x}) = r_{\hat{\ell}}$. The index $\hat{\ell} \in \{1, \cdots, L\}$ can be obtained by maximum a posteriori (MAP) criterion as

$$\hat{\ell} = \arg\max_{k=1,\ldots,L} \Pr\left(X = r_k \mid \hat{X} = r_\ell\right) \tag{32}$$

$$= \arg\max_{k=1,\ldots,L} \Pr\left(X = r_k\right) \Pr\left(\hat{X} = r_\ell \mid X = r_k\right) \tag{33}$$

$$= \arg\max_{k=1,\ldots,L} p_k \left\{ P_H\left(\frac{\sqrt{\Delta}}{\alpha^*}(r_\ell - r_k) + \frac{Q_{\ell+1}}{\beta^*}\right) - P_H\left(\frac{\sqrt{\Delta}}{\alpha^*}(r_\ell - r_k) + \frac{Q_\ell}{\beta^*}\right)\right\} \tag{34}$$

when $\hat{x} = r_\ell$ by using (29), and

$$\hat{\ell} = \arg\max_{k=1,\ldots,L} \Pr\left(X = r_k \mid \hat{X} = \hat{x}\right) \tag{35}$$

$$= \arg\max_{k=1,\ldots,L} \Pr\left(X = r_k\right) p_{\hat{X}|X=r_k}(\hat{x}) \tag{36}$$

$$= \arg\max_{k=1,\ldots,L} p_k p_H\left(\frac{\sqrt{\Delta}}{\alpha^*}\left\{\mathrm{prox}^{-1}_{\frac{\alpha^*}{\beta^*\sqrt{\Delta}}f}(\hat{x}) - r_k\right\}\right) \tag{37}$$

when $\hat{x} \notin \mathcal{R}$ by using (30). When we use the above $\mathcal{Q}_{\mathrm{AO}}(\cdot)$ as the quantizer, the asymptotic SER in (20) can be written as

$$\mathrm{SER}_{\mathrm{AO}} = 1 - \sum_{\ell=1}^{L} p_\ell \Pr\left(\hat{X} \in \mathcal{Q}_{\mathrm{AO}}^{-1}(r_\ell) \mid X = r_\ell\right) \tag{38}$$

$$= 1 - \sum_{\ell=1}^{L} p_\ell \mu_{\hat{X}|X=r_\ell}\left(\mathcal{Q}_{\mathrm{AO}}^{-1}(r_\ell)\right) \tag{39}$$

in general, where we define

$$\mathcal{Q}_{\mathrm{AO}}^{-1}(r_\ell) = \{\hat{x} \mid \mathcal{Q}_{\mathrm{AO}}(\hat{x}) = r_\ell\} \tag{40}$$

and $\mu_{\hat{X}|X=r_\ell}$ denotes the distribution of $\hat{X}$ conditioned on $X = r_\ell$, i.e., the distribution of $\mathrm{prox}_{\frac{\alpha^*}{\beta^*\sqrt{\Delta}}f}\left(r_\ell + \frac{\alpha^*}{\sqrt{\Delta}}H\right)$. Note that the CDF corresponding to $\mu_{\hat{X}|X=r_\ell}$ is given by

$$P_{\hat{X}|X=r_\ell}(\hat{x}) = P_H\left(\frac{\sqrt{\Delta}}{\alpha^*}\left\{\mathrm{prox}^{-1}_{\frac{\alpha^*}{\beta^*\sqrt{\Delta}}f}(\hat{x}) - r_\ell\right\}\right) \tag{41}$$

as shown in (26). Once $\mathcal{Q}_{\mathrm{AO}}^{-1}(r_\ell)$ is obtained, we can compute the asymptotic SER from (39) and (41).

The asymptotically optimal quantizer $\mathcal{Q}_{\mathrm{AO}}(\cdot)$ given by (34) and (37) is usually expressed as a simpler form in practice. Since the estimate $\hat{x} = r_\ell$ should be mapped to the same value as $\mathcal{Q}_{\mathrm{AO}}(r_\ell) = r_\ell$, the quantizer should be written as

$$\mathcal{Q}_{\mathrm{AO}}(\hat{x}) = \begin{cases} r_1 & (\hat{x} < \kappa_2^*) \\ \vdots & \vdots \\ r_\ell & (\kappa_\ell^* \le \hat{x} < \kappa_{\ell+1}^*) \\ \vdots & \vdots \\ r_L & (\kappa_L^* \le \hat{x}) \end{cases}, \tag{42}$$

where $-\infty = \kappa_1^* < \kappa_2^* < \cdots < \kappa_L^* < \kappa_{L+1}^* = \infty$ and $r_{\ell-1} < \kappa_\ell^* < r_\ell$ $(\ell = 2, \ldots, L)$. In this case, we have

$\mathcal{Q}_{\mathrm{AO}}^{-1}(r_\ell) = [\kappa_\ell^*, \kappa_{\ell+1}^*)$ and hence the asymptotic SER in (39) can be written as

$$\widetilde{\mathrm{SER}}_{\mathrm{AO}} = 1 - \sum_{\ell=1}^{L} p_\ell \left\{ P_H\left(\frac{\sqrt{\Delta}}{\alpha^*}(\kappa_{\ell+1}^* - r_\ell) + \frac{Q_{\ell+1}}{\beta^*}\right) - P_H\left(\frac{\sqrt{\Delta}}{\alpha^*}(\kappa_\ell^* - r_\ell) + \frac{Q_\ell}{\beta^*}\right)\right\} \quad (43)$$

by using (27) and (41).

We here mention the computational complexity to perform the asymptotically optimal quantization with $\mathcal{Q}_{\mathrm{AO}}(\cdot)$. For fixed parameters $q_1, \ldots, q_L$, the dominant part of the quantization is to compute α^* and β^* in Theorem III.1. As we will see in Section IV-C, the function $F(\alpha, \beta)$ in (14) is convex-concave. Hence, α^* and β^* can be calculated by searching techniques such as the ternary search and the golden-section search [47]. Since the search in each dimension requires $\mathcal{O}\left(\log \frac{1}{\varepsilon_{\mathrm{tol}}}\right)$ evaluations of $F(\alpha, \beta)$, the whole computational complexity to obtain α^* and β^* is $\mathcal{O}\left(\left(\log \frac{1}{\varepsilon_{\mathrm{tol}}}\right)^2\right)$, where $\varepsilon_{\mathrm{tol}}$ is the error tolerance. The complexity is not problematic in our simulations using the ternary search with $\varepsilon_{\mathrm{tol}} = 10^{-6}$. Once we obtain α^* and β^*, we can compute $\mathcal{Q}_{\mathrm{AO}}(\cdot)$ according to (34) and (37). When $\mathcal{Q}_{\mathrm{AO}}(\cdot)$ can be written as (42), we can perform the quantization more easily by calculating $\kappa_2^*, \ldots, \kappa_L^*$ in advance (See Examples III.1 and III.2 in Section III-E).

E. Proposed Parameter Selection for Box-SOAV

The parameters q_ℓ ($\ell = 1, \ldots, L$) in the Box-SOAV optimization (9) affects the performance of the reconstruction. From the results of the previous subsections, once the parameters q_ℓ are fixed, the asymptotic SER of Box-SOAV with the asymptotically optimal quantizer can be evaluated as follows:

1) Calculate α^* and β^* in Theorem III.1. (Note that the knowledge of the noise variance σ_{v}^2 is required.)
2) Obtain the asymptotically optimal quantizer $\mathcal{Q}_{\mathrm{AO}}(\cdot)$ based on (34) and (37).
3) Compute the asymptotic SER in (20) (or (43) in many cases).

We thus propose the approach to determine the parameters q_ℓ (or Q_ℓ in (11)) by numerically minimizing the resultant asymptotic SER in (20). If the noise variance is known, we can optimize the parameters in the Box-SOAV optimization in terms of the asymptotic SER. Even if the noise variance is unknown, we can use the same approach by estimating the SNR in some manner such as [48]. Although the SNR estimation method in [48] requires that the unknown vector has zero-mean, this assumption is reasonable in many applications such as the signal detection in MIMO communications.

F. Examples of the Analysis

In the following examples, we show the theoretical result for three specific scenarios.

Example III.1 (Binary Vector)**.** We consider the reconstruction of the binary vector $\boldsymbol{x} \in \{r_1, r_2\}^N$. When the estimate $\hat{x}$ of an element of $\boldsymbol{x}$ equals r_1 or r_2, we should just quantize it on the basis of (34). For $\hat{x} \in (r_1, r_2)$, the output of the asymptotically optimal quantizer is determined from (37). We thus obtain the value of κ_2^* such that

$$p_1 p_H\left(\frac{\sqrt{\Delta}}{\alpha^*}\left\{\mathrm{prox}_{\frac{\alpha^*}{\beta^*\sqrt{\Delta}}f}^{-1}(\kappa_2^*) - r_1\right\}\right) = p_2 p_H\left(\frac{\sqrt{\Delta}}{\alpha^*}\left\{\mathrm{prox}_{\frac{\alpha^*}{\beta^*\sqrt{\Delta}}f}^{-1}(\kappa_2^*) - r_2\right\}\right). \quad (44)$$

If the solution of (44) lies in (r_1, r_2), we have

$$\kappa_2^* = \mathrm{prox}_{\frac{\alpha^*}{\beta^*\sqrt{\Delta}}f}\left(\frac{1}{2}(r_1 + r_2) + \frac{(\alpha^*)^2}{\Delta}\frac{1}{r_2 - r_1}\log\frac{p_1}{p_2}\right). \quad (45)$$

In this case, the asymptotically optimal quantizer can be written as

$$\mathcal{Q}_{\mathrm{AO}}(\hat{x}) = \begin{cases} r_1 & (\hat{x} < \kappa_2^*) \\ r_2 & (\kappa_2^* \le \hat{x}) \end{cases} \quad (46)$$

for $\hat{x} \in (r_1, r_2)$. Figure 4 shows an example of the asymptotic density of the estimates by Box-SOAV given by (31). In the figure, we set $\Delta = 0.6$, $(p_1, p_2) = (0.3, 0.7)$, $(r_1, r_2) = (-1, 1)$, $(q_1, q_2) = (0.5, 0.5)$, and SNR of 15 dB. We can see that a certain probability mass is located at $\hat{x} = \pm 1$. The functions $p_k p_{\hat{X}|X=r_k}(\hat{x})$ $(k = 1, 2)$ are also plotted by the dotted lines in the figure. We can confirm that the two curves cross at $\hat{x} = \kappa_2^*$.

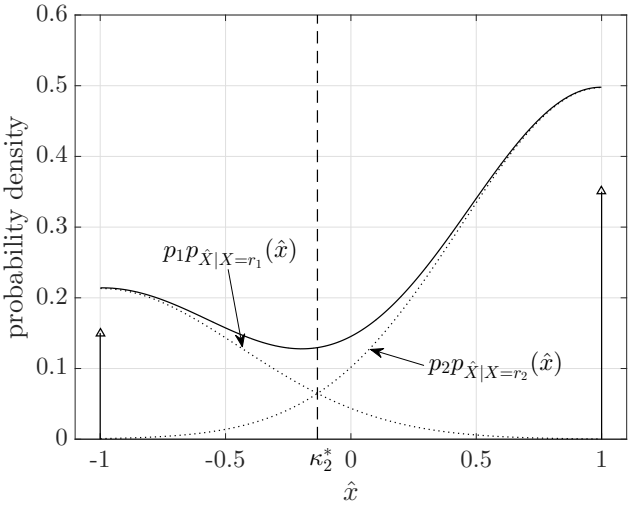

Fig. 4: The asymptotic density (solid line) of the estimates by Box-SOAV and the threshold κ_2^* of the asymptotically optimal quantizer ($\Delta = 0.6$, $(p_1, p_2) = (0.3, 0.7)$, $(r_1, r_2) = (-1, 1)$, $(q_1, q_2) = (0.5, 0.5)$, SNR $= 15$ dB)

We can obtain the asymptotically optimal parameters of the Box-SOAV optimization from the theoretical result. For the reconstruction of $\boldsymbol{x} \in \{r_1, r_2\}^N$, the Box-SOAV optimization

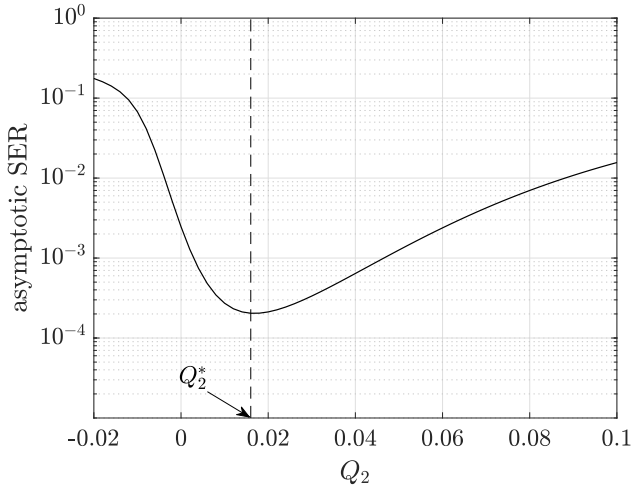

Fig. 5: Asymptotic SER of $\mathcal{Q}_{\mathrm{AO}}(\cdot)$ versus Q_2 ($\Delta = 0.7$, $(r_1, r_2) = (0, 1)$, $(p_1, p_2) = (0.8, 0.2)$, SNR $= 15$ dB)

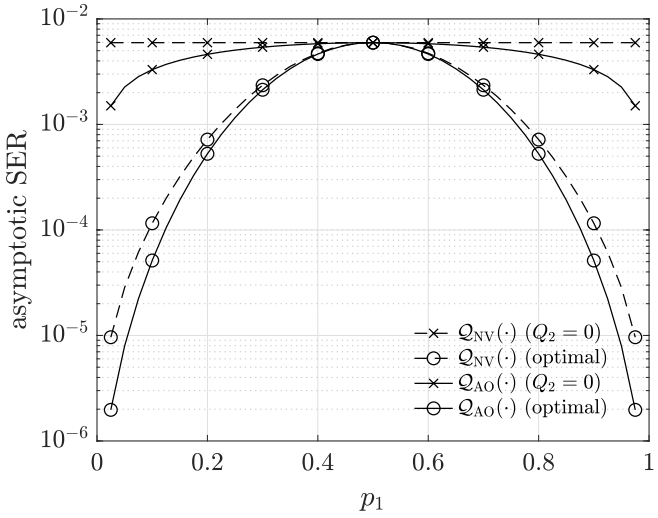

Fig. 6: Asymptotic SER versus p_1 for binary vector ($\Delta = 0.7$, $(r_1, r_2) = (-1, 1)$, SNR $= 15$ dB)

is given by

$$\hat{\boldsymbol{x}} = \arg\min_{\boldsymbol{s}\in[r_1,r_2]^N} \left\{ \frac{1}{2}\left\|\boldsymbol{y}-\boldsymbol{A}\boldsymbol{s}\right\|_2^2 + q_1\left\|\boldsymbol{s}-r_1\mathbf{1}\right\|_1 + q_2\left\|\boldsymbol{s}-r_2\mathbf{1}\right\|_1 \right\} \quad (47)$$

$$= \arg\min_{\boldsymbol{s}\in[r_1,r_2]^N} \left\{ \frac{1}{2}\left\|\boldsymbol{y}-\boldsymbol{A}\boldsymbol{s}\right\|_2^2 + Q_2\sum_{n=1}^{N} s_n \right\} \quad (48)$$

because $q_1\left\|\boldsymbol{s}-r_1\mathbf{1}\right\|_1 + q_2\left\|\boldsymbol{s}-r_2\mathbf{1}\right\|_1 = Q_2\sum_{n=1}^N s_n +$ (const.) for $\boldsymbol{s}\in[r_1,r_2]^N$. Hence, the performance of Box-SOAV depends only on Q_2. By numerically computing the value of Q_2 minimizing the asymptotic SER, we can obtain the optimal $\mathcal{Q}_{\mathrm{AO}}(\cdot)$ and the corresponding asymptotic SER. For example, Fig. 5 shows the asymptotic SER of $\mathcal{Q}_{\mathrm{AO}}(\cdot)$ versus Q_2 when $\Delta = 0.7$, $(r_1, r_2) = (0, 1)$, $(p_1, p_2) = (0.8, 0.2)$, and SNR of 15 dB. From the figure, we can see that the asymptotic performance of Box-SOAV largely depends on the parameter Q_2. By using the optimal value Q_2^* of Q_2 minimizing the asymptotic SER, we can obtain the asymptotically optimal values of α^*, β^*, and κ_2^* in (45).

We then compare the performance of quantizer $\mathcal{Q}_{\mathrm{NV}}(\cdot)$ in (21) and $\mathcal{Q}_{\mathrm{AO}}(\cdot)$ in (46). Figure 6 shows the asymptotic SER of Box-SOAV with four cases: (i) $\mathcal{Q}_{\mathrm{NV}}(\cdot)$ with $Q_2 = 0$, (ii) $\mathcal{Q}_{\mathrm{NV}}(\cdot)$ with the optimal Q_2, (iii) $\mathcal{Q}_{\mathrm{AO}}(\cdot)$ with $Q_2 = 0$, and (iv) $\mathcal{Q}_{\mathrm{AO}}(\cdot)$ with the proposed optimal parameter selection. In the figure, we set $\Delta = 0.7$, $(r_1, r_2) = (-1, 1)$, and SNR of 15 dB. The figure shows that the proposed optimal parameter selection can achieve better performance than the naive selection $Q_2 = 0$. Moreover, the performance of $\mathcal{Q}_{\mathrm{AO}}(\cdot)$ is better than that of $\mathcal{Q}_{\mathrm{NV}}(\cdot)$, especially when the difference between p_1 and p_2 is large. We can also see that $\mathcal{Q}_{\mathrm{NV}}(\cdot)$ and $\mathcal{Q}_{\mathrm{AO}}(\cdot)$ have the same performance when $p_1 = p_2 = 0.5$. In other words, the quantization to the nearest candidate r_ℓ is optimal when the distribution is uniform. This fact can also be derived from (45), which results in $\kappa_2^* = (r_1 + r_2)/2$ when $p_1 = p_2 = 0.5$ and $q_1 = q_2$.

Example III.2 (Discrete-Valued Sparse Vector)**.** The discrete-valued vector $\boldsymbol{x}$ with $(p_1, p_2, p_3) = ((1-p_0)/2, p_0, (1-p_0)/2)$ and $(r_1, r_2, r_3) = (-r, 0, r)$ $(r > 0)$ becomes sparse when p_0 is large. By a similar discussion to Example III.1, the asymptotically optimal quantizer is given by

$$\mathcal{Q}_{\mathrm{AO}}(\hat{x}) = \begin{cases} -r & (\hat{x} < \kappa_2^*) \\ 0 & (\kappa_2^* \le \hat{x} < \kappa_3^*) \\ r & (\kappa_3^* \le \hat{x}) \end{cases} \quad (49)$$

when $-r < \kappa_2^* < 0$, where

$$\kappa_2^* = \mathrm{prox}_{\frac{\alpha^*}{\beta^*\sqrt{\Delta}} f}\left(-\frac{1}{2}r + \frac{(\alpha^*)^2}{\Delta}\frac{1}{r}\log\frac{1-p_0}{2p_0}\right), \quad (50)$$

$$\kappa_3^* = -\kappa_2^*. \quad (51)$$

For the reconstruction of $\boldsymbol{x}$ via Box-SOAV in this scenario, we can set $q_1 = q_3$ from the symmetry of the distribution. As a result, the Box-SOAV optimization problem can be written as

$$\hat{\boldsymbol{x}} = \arg\min_{\boldsymbol{s}\in[-r,r]^N} \left\{ \frac{1}{2}\left\|\boldsymbol{y}-\boldsymbol{A}\boldsymbol{s}\right\|_2^2 + q_1\left\|\boldsymbol{s}+r\mathbf{1}\right\|_1 + q_2\left\|\boldsymbol{s}\right\|_1 + q_1\left\|\boldsymbol{s}-r\mathbf{1}\right\|_1 \right\} \quad (52)$$

$$= \arg\min_{\boldsymbol{s}\in[-r,r]^N} \left\{ \frac{1}{2}\left\|\boldsymbol{y}-\boldsymbol{A}\boldsymbol{s}\right\|_2^2 + q_2\left\|\boldsymbol{s}\right\|_1 \right\} \quad (53)$$

because $q_1\left\|\boldsymbol{s}+r\mathbf{1}\right\|_1 + q_1\left\|\boldsymbol{s}-r\mathbf{1}\right\|_1 = 2q_1rN =$ (const.) for $\boldsymbol{s}\in[-r,r]^N$. Hence, only q_2 is the parameter to be optimized. Note that the Box-SOAV optimization problem is equivalent to Box-LASSO [28] in this case.

We show several asymptotic results for the reconstruction of the vector with $(p_1, p_2, p_3) = ((1-p_0)/2, p_0, (1-p_0)/2)$ and $(r_1, r_2, r_3) = (-r, 0, r)$ $(r > 0)$. We firstly discuss the sensitivity of $\mathcal{Q}_{\mathrm{AO}}(\cdot)$ in Fig. 7, which shows κ_2^* in (50) as the function of p_0. In the figure, we set $(p_1, p_2, p_3) = ((1-p_0)/2, p_0, (1-p_0)/2)$, $(r_1, r_2, r_3) = (-1, 0, 1)$, and the SNR of 15 dB. The parameter q_2 is numerically chosen by

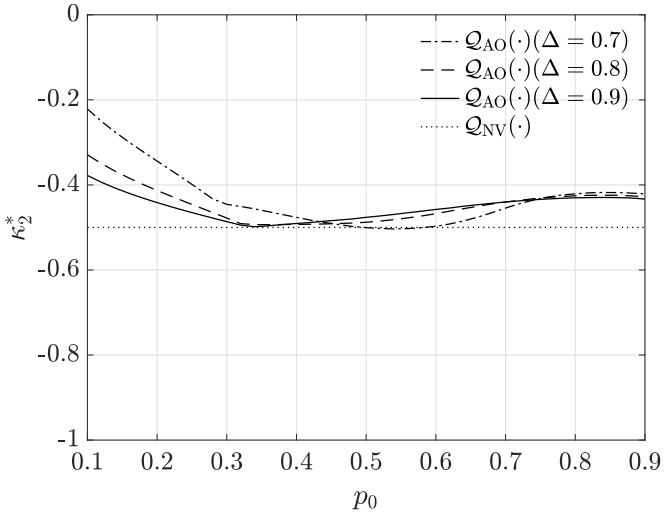

Fig. 7: Sensitivity of κ_2^* against the change of p_0 ($(p_1,p_2,p_3) = ((1-p_0)/2, p_0, (1-p_0)/2)$, $(r_1,r_2,r_3) = (-1,0,1)$, SNR $= 15$ dB)

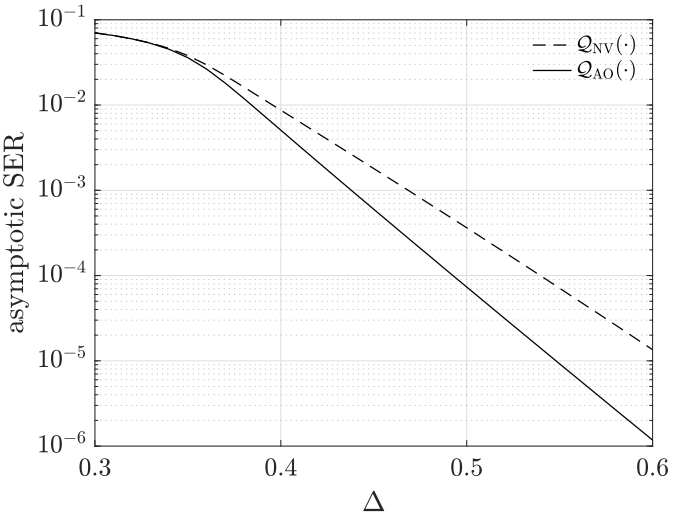

Fig. 8: Asymptotic SER versus $\Delta = M/N$ for discrete-valued sparse vector ($(p_1,p_2,p_3) = (0.05, 0.9, 0.05)$, $(r_1,r_2,r_3) = (-1,0,1)$, SNR $= 15$ dB)

minimizing the asymptotic SER. We can see that the value of κ_2^* does not change so significantly, especially for large p_0. However, since κ_2^* is different from the threshold -0.5 of $\mathcal{Q}_{\rm NV}(\cdot)$, we can improve the asymptotic performance by using $\mathcal{Q}_{\rm AO}(\cdot)$ with κ_2^* instead of $\mathcal{Q}_{\rm NV}(\cdot)$. Next, we show the performance gain obtained by using $\mathcal{Q}_{\rm AO}(\cdot)$. Figure 8 shows the asymptotic SER of Box-SOAV with $\mathcal{Q}_{\rm NV}(\cdot)$ and $\mathcal{Q}_{\rm AO}(\cdot)$. In the figure, we set $(p_1,p_2,p_3) = (0.05, 0.9, 0.05)$, $(r_1,r_2,r_3) = (-1,0,1)$, and SNR of 15 dB. The parameter q_2 of Box-SOAV is numerically chosen by minimizing the asymptotic SER for each quantizer. We can observe that the asymptotically optimal quantizer $\mathcal{Q}_{\rm AO}(\cdot)$ outperforms $\mathcal{Q}_{\rm NV}(\cdot)$ especially for large $\Delta = M/N$. Although the estimate $\hat{\boldsymbol{x}}$ itself is the same for Box-SOAV and Box-LASSO irrespective of the quantizer, the optimization of the quantizer improves the asymptotic SER performance. Finally, in Fig. 9, we compare the performance of Box-SOAV with the matched filter bound

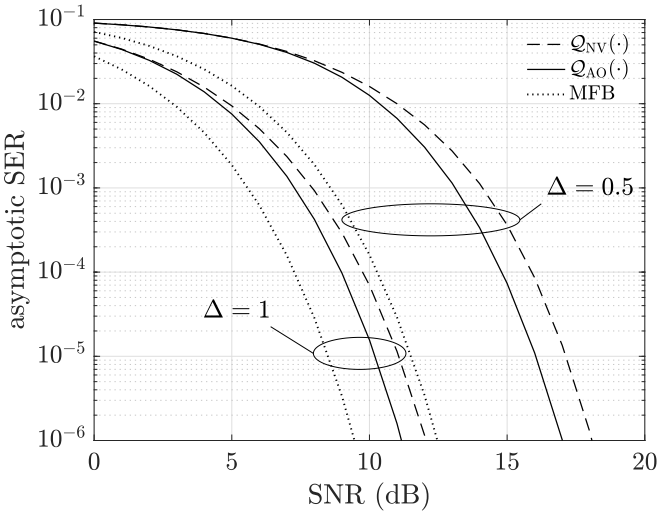

Fig. 9: Performance comparison between Box-SOAV and MFB ($(p_1,p_2,p_3) = (0.05, 0.9, 0.05)$, $(r_1,r_2,r_3) = (-1,0,1)$, $\Delta = 0.7$)

(MFB), which is defined as the probability of the estimation error for $x_n \in \{r_1,\dots,r_L\}$ from

$$y_{\rm MFB} \coloneqq \boldsymbol{a}_n^{\mathsf{T}}\left(\boldsymbol{y} - \sum_{n'\neq n}\boldsymbol{a}_{n'}x_{n'}\right) \tag{54}$$

$$= \|\boldsymbol{a}_n\|_2^2\, x_n + \boldsymbol{a}_n^{\mathsf{T}}\boldsymbol{v} \tag{55}$$

when $x_{n'}$ ($n' \neq n$) is known. Note that $\|\boldsymbol{a}_n\|_2^2 \xrightarrow{\rm P} \Delta$ and $\boldsymbol{a}_n^{\mathsf{T}}\boldsymbol{v} \sim \mathcal{N}(0, \Delta\sigma_{\rm v}^2)$ in the asymptotic regime, where $\mathcal{N}(\mu,\sigma^2)$ denotes the Gaussian distribution with mean μ and variance σ^2. When $(p_1,p_2,p_3) = ((1-p_0)/2, p_0, (1-p_0)/2)$ and $(r_1,r_2,r_3) = (-1,0,1)$, the asymptotic MFB is given by

$$\begin{aligned}&{\rm SER}_{\rm MFB}\\ &= 1 - \left[(1-p_0)P_H\left(\frac{\Delta+\tilde{\kappa}_2}{\sqrt{\Delta\sigma_{\rm v}^2}}\right)\right.\\ &\qquad \left. + p_0\left\{P_H\left(-\frac{\tilde{\kappa}_2}{\sqrt{\Delta\sigma_{\rm v}^2}}\right) - P_H\left(\frac{\tilde{\kappa}_2}{\sqrt{\Delta\sigma_{\rm v}^2}}\right)\right\}\right],\end{aligned} \tag{56}$$

where

$$\tilde{\kappa}_2 = \sigma_{\rm v}^2 \log\frac{1-p_0}{2p_0} - \frac{\Delta}{2}. \tag{57}$$

The asymptotic SER in (56) can be derived by considering the MAP estimation of x_n from $y_{\rm MFB}$ and the asymptotically optimal quantizer designed for the MAP estimation. From Fig. 9, we observe that the asymptotic SER of $\mathcal{Q}_{\rm AO}(\cdot)$ is closer to the MFB than that of $\mathcal{Q}_{\rm NV}(\cdot)$. The figure also shows that the difference from the MFB becomes smaller as the measurement ratio Δ increases.

Example III.3 (Uniformly distributed vector)**.** The analysis in [49] suggests that we should remove the SOAV regularizer (i.e., $q_1 = \cdots = q_L = 0$) and use only the box constraint for the uniformly distributed vector with $p_1 = \cdots = p_L = 1/L$ (See also Remark III.1). As shown below, the quantization by $\mathcal{Q}_{\rm NV}(\cdot)$ to the nearest value is asymptotically optimal in

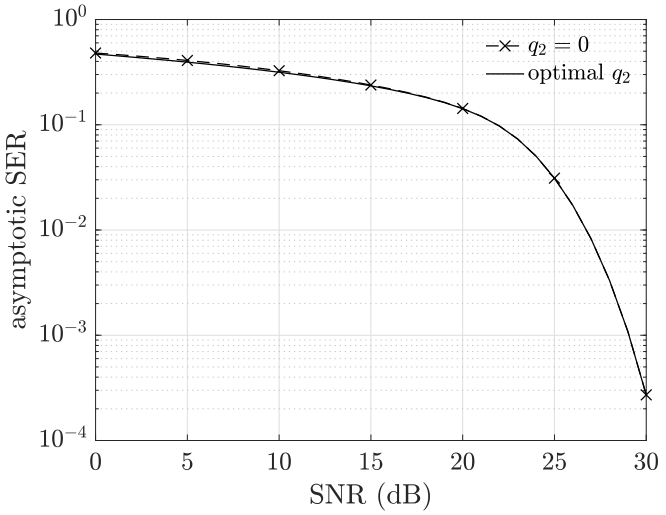

Fig. 10: Asymptotic SER for the uniform distribution ($(p_1, p_2, p_3) = (1/3, 1/3, 1/3)$, $(r_1, r_2, r_3) = (-1, 0, 1)$, $\Delta = 0.7$)

this case. In the same manner as Example III.1, the optimal threshold κ_ℓ^* ($\ell = 2, \ldots, L$) should satisfy

$$p_{\ell-1} p_H \left(\frac{\sqrt{\Delta}}{\alpha^*} \left\{ \mathrm{prox}^{-1}_{\frac{\alpha^*}{\beta^* \sqrt{\Delta}} f} \left(\kappa_\ell^* \right) - r_{\ell-1} \right\} \right) = p_\ell p_H \left(\frac{\sqrt{\Delta}}{\alpha^*} \left\{ \mathrm{prox}^{-1}_{\frac{\alpha^*}{\beta^* \sqrt{\Delta}} f} \left(\kappa_\ell^* \right) - r_\ell \right\} \right), \tag{58}$$

which can be rewritten as

$$\kappa_\ell^* = \frac{1}{2} \left(r_{\ell-1} + r_\ell \right) \tag{59}$$

because $p_{\ell-1} = p_\ell$ and $q_1 = \cdots = q_L = 0$. The threshold (59) means that the asymptotically optimal quantizer $\mathcal{Q}_{\mathrm{AO}}(\cdot)$ becomes equivalent to $\mathcal{Q}_{\mathrm{NV}}(\cdot)$.

Strictly speaking, however, the removal of the SOAV regularizer and the use of $\mathcal{Q}_{\mathrm{NV}}(\cdot)$ are not necessarily optimal even for the uniform distribution in terms of the asymptotic SER. In fact, Fig. 7 shows that the value of κ_2^* for $\Delta = 0.7$ is different from the threshold -0.5 of $\mathcal{Q}_{\mathrm{NV}}(\cdot)$ when $p_0 = 1/3$, which means the uniform distribution $(p_1, p_2, p_3) = (1/3, 1/3, 1/3)$. This means that $q_2 = 0$ and the naive quantizer $\mathcal{Q}_{\mathrm{NV}}(\cdot)$ are not asymptotically optimal in this case. However, $\mathcal{Q}_{\mathrm{NV}}(\cdot)$ and $\mathcal{Q}_{\mathrm{AO}}(\cdot)$ have almost the same asymptotic performance as shown in Fig. 10. In the figure, we show the asymptotic performance of $\mathcal{Q}_{\mathrm{NV}}(\cdot)$ with $q_2 = 0$ and $\mathcal{Q}_{\mathrm{AO}}(\cdot)$ with the optimal q_2 for $(p_1, p_2, p_3) = (1/3, 1/3, 1/3)$, $(r_1, r_2, r_3) = (-1, 0, 1)$, and $\Delta = 0.7$. Hence, we can obtain almost the best performance by using the naive quantizer $\mathcal{Q}_{\mathrm{NV}}(\cdot)$ with $q_2 = 0$ in this case.

Remark III.1. In [49], a parameter selection method has been proposed for the SOAV optimization on the basis of the analysis of the discreteness-aware approximate message passing (DAMP) algorithm. However, the method does not necessarily minimize the SER of the SOAV optimization because it minimizes the required number of measurements for the perfect reconstruction in the noise-free case. Since it does not take the noise variance into consideration, it is difficult to fairly compare the result in [49] with the theoretical result in this paper.

IV. Proof of Theorem III.1

In this section, we show the proof of Theorem III.1. Although the procedure of the proof roughly follows the analysis using CGMT in the literature (e.g., [23], [24]), we need to modify several parts for our problem. The difference from the SER analysis for the box relaxation method in [23] mainly comes from the fact that we use the regularization term in the Box-SOAV optimization. Moreover, since we consider general discrete distribution $p_1, \ldots, p_L$, we need to design the set $\mathcal{S}$ in CGMT appropriately. In the proof, we mention the main differences as necessary.

A. (PO)

To obtain the (PO) problem for the proof, we firstly define the error vector as $\boldsymbol{w} \coloneqq \boldsymbol{s} - \boldsymbol{x}$ and rewrite the Box-SOAV optimization (9) as

$$\min_{\boldsymbol{w} \in \mathcal{S}_{\mathrm{w}}} \frac{1}{N} \left\{ \frac{1}{2} \left\| \boldsymbol{A}\boldsymbol{w} - \boldsymbol{v} \right\|_2^2 + \sum_{\ell=1}^{L} q_\ell \left\| \boldsymbol{x} + \boldsymbol{w} - r_\ell \boldsymbol{1} \right\|_1 \right\}, \tag{60}$$

where $\mathcal{S}_{\mathrm{w}} = \left\{ \boldsymbol{z} \in \mathbb{R}^N \mid r_1 - x_n \le z_n \le r_L - x_n \ (n = 1, \ldots, N) \right\}$ and the objective function is normalized by N. Since we have used the box constraint $\boldsymbol{s} \in [r_1, r_L]^N$ in the original Box-SOAV optimization (9), the constraint set $\mathcal{S}_{\mathrm{w}}$ becomes the closed compact set. As denoted in Theorem II.1, $\mathcal{S}_{\mathrm{w}}$ is required to be a closed compact set to apply CGMT. If we do not use the box constraint, we need to treat the boundedness of the error vector in some other way as in [24, Appendix A]. Compared to that, the box constraint in the Box-SOAV optimization will be reasonable and simplify the proof for the boundedness of the constraint set. Unlike the case with the box relaxation method [23], we have the regularization term $\sum_{\ell=1}^{L} q_\ell \left\| \boldsymbol{x} + \boldsymbol{w} - r_\ell \boldsymbol{1} \right\|_1$ in the objective function. Thus, we cannot take the same approach as in [23] to transform the optimization problem (60). To tackle this problem, we transform (60) in accordance with [24], which utilizes a slightly different approach from [23]. Specifically, since the convex conjugate of the function $\xi(\boldsymbol{z}) \coloneqq \frac{1}{2} \left\| \boldsymbol{z} \right\|_2^2$ is given by

$$\xi^*(\boldsymbol{z}^*) \coloneqq \max_{\boldsymbol{u} \in \mathbb{R}^M} \left\{ \boldsymbol{u}^{\mathsf{T}} \boldsymbol{z}^* - \frac{1}{2} \left\| \boldsymbol{u} \right\|_2^2 \right\} \tag{61}$$

$$= \frac{1}{2} \left\| \boldsymbol{z}^* \right\|_2^2, \tag{62}$$

we have

$$\frac{1}{2} \left\| \boldsymbol{A}\boldsymbol{w} - \boldsymbol{v} \right\|_2^2 = \max_{\boldsymbol{u} \in \mathbb{R}^M} \left\{ \sqrt{N} \boldsymbol{u}^{\mathsf{T}} \left(\boldsymbol{A}\boldsymbol{w} - \boldsymbol{v} \right) - \frac{N}{2} \left\| \boldsymbol{u} \right\|_2^2 \right\}. \tag{63}$$

Hence, the optimization problem (60) is equivalent to

$$\min_{\boldsymbol{w} \in \mathcal{S}_{\mathrm{w}}} \max_{\boldsymbol{u} \in \mathbb{R}^M} \frac{1}{N} \left\{ \sqrt{N} \boldsymbol{u}^{\mathsf{T}} \left(\boldsymbol{A}\boldsymbol{w} - \boldsymbol{v} \right) - \frac{N}{2} \left\| \boldsymbol{u} \right\|_2^2 + \sum_{\ell=1}^{L} q_\ell \left\| \boldsymbol{x} + \boldsymbol{w} - r_\ell \boldsymbol{1} \right\|_1 \right\}. \tag{64}$$

Let $\boldsymbol{w}^*$ and $\boldsymbol{u}^*$ be the optimal values of $\boldsymbol{w}$ and $\boldsymbol{u}$, respectively. Since $\boldsymbol{u}^*$ satisfies $\boldsymbol{u}^* = \frac{1}{\sqrt{N}}(\boldsymbol{A}\boldsymbol{w}^* - \boldsymbol{v})$ and $\boldsymbol{w}^*$ is bounded, there exists a constant C_{u} such that $\|\boldsymbol{u}^*\|_2 \leq C_{\mathrm{u}}$ with probability approaching 1. We can thus rewrite (64) as

$$\min_{\boldsymbol{w}\in\mathcal{S}_{\mathrm{w}}}\max_{\boldsymbol{u}\in\mathcal{S}_{\mathrm{u}}}\left\{\frac{1}{N}\boldsymbol{u}^{\mathsf{T}}\left(\sqrt{N}\boldsymbol{A}\right)\boldsymbol{w} - \frac{1}{\sqrt{N}}\boldsymbol{v}^{\mathsf{T}}\boldsymbol{u} - \frac{1}{2}\|\boldsymbol{u}\|_2^2 + \frac{1}{N}\sum_{\ell=1}^{L} q_\ell \|\boldsymbol{x}+\boldsymbol{w}-r_\ell\boldsymbol{1}\|_1\right\}, \tag{65}$$

where $\mathcal{S}_{\mathrm{u}} = \left\{\boldsymbol{z}\in\mathbb{R}^M \mid \|\boldsymbol{z}\|_2 \leq C_{\mathrm{u}}\right\}$. The optimization problem (65) takes the form of (PO) in (6).

B. (AO)

We then analyze the (AO) problem corresponding to (65). We can confirm that $\mathcal{S}_{\mathrm{w}}$ and $\mathcal{S}_{\mathrm{u}}$ are closed compact sets and the function $-\frac{1}{\sqrt{N}}\boldsymbol{v}^{\mathsf{T}}\boldsymbol{u} - \frac{1}{2}\|\boldsymbol{u}\|_2^2 + \frac{1}{N}\sum_{\ell=1}^{L} q_\ell \|\boldsymbol{x}+\boldsymbol{w}-r_\ell\boldsymbol{1}\|_1$ is convex-concave on $\mathcal{S}_{\mathrm{w}}\times\mathcal{S}_{\mathrm{u}}$. Hence, the (AO) problem corresponding to (65) is given by

$$\min_{\boldsymbol{w}\in\mathcal{S}_{\mathrm{w}}}\max_{\boldsymbol{u}\in\mathcal{S}_{\mathrm{u}}}\left\{\frac{1}{N}\left(\|\boldsymbol{w}\|_2\boldsymbol{g}^{\mathsf{T}}\boldsymbol{u} - \|\boldsymbol{u}\|_2\boldsymbol{h}^{\mathsf{T}}\boldsymbol{w}\right) - \frac{1}{\sqrt{N}}\boldsymbol{v}^{\mathsf{T}}\boldsymbol{u} - \frac{1}{2}\|\boldsymbol{u}\|_2^2 + \frac{1}{N}\sum_{\ell=1}^{L} q_\ell \|\boldsymbol{x}+\boldsymbol{w}-r_\ell\boldsymbol{1}\|_1\right\}, \tag{66}$$

which can be rewritten as

$$\min_{\boldsymbol{w}\in\mathcal{S}_{\mathrm{w}}}\max_{\boldsymbol{u}\in\mathcal{S}_{\mathrm{u}}}\left\{\frac{1}{\sqrt{N}}\left(\frac{\|\boldsymbol{w}\|_2}{\sqrt{N}}\boldsymbol{g}^{\mathsf{T}} - \boldsymbol{v}^{\mathsf{T}}\right)\boldsymbol{u} - \frac{1}{N}\|\boldsymbol{u}\|_2\boldsymbol{h}^{\mathsf{T}}\boldsymbol{w} - \frac{1}{2}\|\boldsymbol{u}\|_2^2 + \frac{1}{N}\sum_{\ell=1}^{L} q_\ell \|\boldsymbol{x}+\boldsymbol{w}-r_\ell\boldsymbol{1}\|_1\right\}. \tag{67}$$

Since both $\boldsymbol{g}$ and $\boldsymbol{v}$ are Gaussian, $\frac{\|\boldsymbol{w}\|_2}{\sqrt{N}}\boldsymbol{g} - \boldsymbol{v}$ is also Gaussian distributed with mean $\boldsymbol{0}$ and covariance matrix $\left(\frac{\|\boldsymbol{w}\|_2^2}{N} + \sigma_{\mathrm{v}}^2\right)\boldsymbol{I}$. We can thus rewrite $\left(\frac{\|\boldsymbol{w}\|_2}{\sqrt{N}}\boldsymbol{g}^{\mathsf{T}} - \boldsymbol{v}^{\mathsf{T}}\right)\boldsymbol{u}$ as $\sqrt{\frac{\|\boldsymbol{w}\|_2^2}{N} + \sigma_{\mathrm{v}}^2}\boldsymbol{g}^{\mathsf{T}}\boldsymbol{u}$ by the slight abuse of notation, where $\boldsymbol{g}$ is the random vector with i.i.d. standard Gaussian elements. By setting $\|\boldsymbol{u}\|_2 = \beta$, the (AO) problem can be further rewritten as

$$\min_{\boldsymbol{w}\in\mathcal{S}_{\mathrm{w}}}\max_{0\leq\beta\leq C_{\mathrm{u}}}\left\{\sqrt{\frac{\|\boldsymbol{w}\|_2^2}{N} + \sigma_{\mathrm{v}}^2}\frac{\beta\|\boldsymbol{g}\|_2}{\sqrt{N}} - \frac{1}{N}\beta\boldsymbol{h}^{\mathsf{T}}\boldsymbol{w} - \frac{1}{2}\beta^2 + \frac{1}{N}\sum_{\ell=1}^{L} q_\ell \|\boldsymbol{x}+\boldsymbol{w}-r_\ell\boldsymbol{1}\|_1\right\}. \tag{68}$$

Note that the optimization of β is difficult here in this case because the resultant optimization problem of α^* becomes complicated, whereas it can be easily done in the case with the box relaxation method [23]. From the identity $\chi = \min_{\alpha>0}\left(\frac{\alpha}{2} + \frac{\chi^2}{2\alpha}\right)$ for χ (>0), we have

$$\sqrt{\frac{\|\boldsymbol{w}\|_2^2}{N} + \sigma_{\mathrm{v}}^2} = \min_{\alpha>0}\left(\frac{\alpha}{2} + \frac{\frac{\|\boldsymbol{w}\|_2^2}{N} + \sigma_{\mathrm{v}}^2}{2\alpha}\right) \tag{69}$$

and rewrite (68) as

$$\max_{\beta>0}\min_{\alpha>0}\left\{\frac{\alpha\beta}{2}\frac{\|\boldsymbol{g}\|_2}{\sqrt{N}} + \frac{\sigma_{\mathrm{v}}^2\beta}{2\alpha}\frac{\|\boldsymbol{g}\|_2}{\sqrt{N}} - \frac{1}{2}\beta^2 - \frac{1}{N}\sum_{n=1}^{N}\frac{\alpha\beta h_n^2}{2}\frac{\sqrt{N}}{\|\boldsymbol{g}\|_2} + \frac{\beta}{\alpha}\frac{\|\boldsymbol{g}\|_2}{\sqrt{N}}\min_{\boldsymbol{w}\in\mathcal{S}_{\mathrm{w}}}\frac{1}{N}\sum_{n=1}^{N} J_n(w_n)\right\}, \tag{70}$$

where

$$J_n(w_n) = \frac{1}{2}\left(w_n - \frac{\sqrt{N}}{\|\boldsymbol{g}\|_2}\alpha h_n\right)^2 + \frac{\alpha}{\beta}\frac{\sqrt{N}}{\|\boldsymbol{g}\|_2}\sum_{\ell=1}^{L} q_\ell \left|x_n + w_n - r_\ell\right|. \tag{71}$$

Note that the objective function becomes separable for w_n in (70), and that the change in the range of β does not change the optimal value. The function $J_n(w_n)$ includes the regularization term $\frac{\alpha}{\beta}\frac{\sqrt{N}}{\|\boldsymbol{g}\|_2}\sum_{\ell=1}^{L} q_\ell |x_n + w_n - r_\ell|$ unlike the case with the box relaxation method [23]. Since the optimization with respect to $\boldsymbol{w}$ in (70) is given by

$$\begin{aligned}&\min_{\boldsymbol{w}\in\mathcal{S}_{\mathrm{w}}}\frac{1}{N}\sum_{n=1}^{N} J_n(w_n)\\ &= \min_{\boldsymbol{s}\in[r_1,r_L]^N}\frac{1}{N}\sum_{n=1}^{N}\left[\frac{1}{2}\left\{s_n - \left(x_n + \frac{\sqrt{N}}{\|\boldsymbol{g}\|_2}\alpha h_n\right)\right\}^2 + \frac{\alpha}{\beta}\frac{\sqrt{N}}{\|\boldsymbol{g}\|_2}\sum_{\ell=1}^{L} q_\ell |s_n - r_\ell|\right] \qquad (72)\\ &= \frac{1}{N}\sum_{n=1}^{N}\mathrm{env}_{\frac{\alpha}{\beta}\frac{\sqrt{N}}{\|\boldsymbol{g}\|_2}f}\left(x_n + \frac{\sqrt{N}}{\|\boldsymbol{g}\|_2}\alpha h_n\right), \qquad (73)\end{aligned}$$

(70) can be rewritten as

$$\phi_N^* = \max_{\beta>0}\min_{\alpha>0} F_N(\alpha,\beta), \tag{74}$$

where

$$\begin{aligned}&F_N(\alpha,\beta)\\ &= \frac{\alpha\beta}{2}\frac{\|\boldsymbol{g}\|_2}{\sqrt{N}} + \frac{\sigma_{\mathrm{v}}^2\beta}{2\alpha}\frac{\|\boldsymbol{g}\|_2}{\sqrt{N}} - \frac{1}{2}\beta^2 - \frac{1}{N}\sum_{n=1}^{N}\frac{\alpha\beta h_n^2}{2}\frac{\sqrt{N}}{\|\boldsymbol{g}\|_2}\\ &\quad + \frac{\beta}{\alpha}\frac{\|\boldsymbol{g}\|_2}{\sqrt{N}}\frac{1}{N}\sum_{n=1}^{N}\mathrm{env}_{\frac{\alpha}{\beta}\frac{\sqrt{N}}{\|\boldsymbol{g}\|_2}f}\left(x_n + \frac{\sqrt{N}}{\|\boldsymbol{g}\|_2}\alpha h_n\right).\end{aligned} \tag{75}$$

The optimal value of $\boldsymbol{w}$ is given by

$$\hat{\boldsymbol{w}}_N(\boldsymbol{h},\boldsymbol{x}) = \mathrm{prox}_{\frac{\alpha_N^*}{\beta_N^*}\frac{\sqrt{N}}{\|\boldsymbol{g}\|_2}f}\left(\boldsymbol{x} + \frac{\sqrt{N}}{\|\boldsymbol{g}\|_2}\alpha_N^*\boldsymbol{h}\right) - \boldsymbol{x}, \tag{76}$$

where α_N^* and β_N^* are the optimal values of α and β corresponding to ϕ_N^*, respectively.

C. Applying CGMT

We then consider the condition (i) of Theorem II.1. As $N\to\infty$, $F_N(\alpha,\beta)$ converges pointwise to $F(\alpha,\beta)$ defined in Theorem III.1. Since we can see from (68) and (69) that $F_N(\alpha,\beta)$ is convex-concave, $F(\alpha,\beta)$ is also convex-concave.

Let $\phi^* = \max_{\beta>0} \min_{\alpha>0} F(\alpha,\beta)$ and denote the optimal values of α and β by α^* and β^*, respectively. By a similar discussion to the proof of [23, Lemma IV. 1], we have $\phi_N^* \xrightarrow{\mathrm{P}} \phi^*$ and $(\alpha_N^*, \beta_N^*) \xrightarrow{\mathrm{P}} (\alpha^*, \beta^*)$ as $N \to \infty$. Hence, the optimal value of (AO) satisfies the condition (i) in CGMT for $\bar{\phi} = \phi^*$ and any $\eta > 0$.

Next, we define the set $\mathcal{S}$ used in CGMT. We have the following lemma for the optimizer $\hat{\boldsymbol{w}}_N$ of (AO) in (76).

Lemma IV.1. For any function $\psi(\cdot,\cdot) \in \mathcal{L}$ (given by (15)), we have

$$\operatorname*{plim}_{N\to\infty} \frac{1}{N}\sum_{n=1}^{N} \psi\left(\hat{w}_{N,n}(h_n, x_n), x_n\right) = \mathrm{E}\left[\psi\left(\hat{X} - X, X\right)\right], \tag{77}$$

where $\hat{w}_{N,n}(h_n, x_n)$ denotes the nth element of $\hat{\boldsymbol{w}}_N$ in (76).

Proof: See Appendix C. ∎

From Lemma IV.1, we can define

$$\mathcal{S} = \left\{ \boldsymbol{z} \in \mathbb{R}^N \;\middle|\; \left| \frac{1}{N}\sum_{n=1}^{N} \psi(z_n, x_n) - \mathrm{E}\left[\psi\left(\hat{X} - X, X\right)\right] \right| < \varepsilon \right\} \tag{78}$$

and obtain $\hat{\boldsymbol{w}}_N(\boldsymbol{h}, \boldsymbol{x}) \in \mathcal{S}$ with probability approaching 1 for any ε (> 0). Note that we define the function $\psi(\cdot,\cdot)$ as a bivariate function of $\hat{X} - X$ and X, whereas it is defined as a univariate function of $\hat{X} - X$ in [23]. This is because we would like to obtain not only the result for the error $\hat{X} - X$ but also that of the estimate $\hat{X}$ as in Corollary III.1 and Theorem III.2. When the intervals of $r_1, \ldots, r_L$ is not uniform unlike PAM signals, we require the distribution of the estimate $\hat{X}$ to obtain the asymptotic SER because the symbol error for x_n depends not only on the error $\hat{x}_n - x_n$ but also on the value of x_n.

Finally, we consider the condition (ii) of CGMT. From the strong convexity in $\boldsymbol{w}$ of the objective function in (68), we can show $\phi_{\mathcal{S}^{\mathrm{c}}} \geq \phi_N^* + \tilde{\eta}$ with probability approaching 1 for a constant $\tilde{\eta}$ (> 0), where $\phi_{\mathcal{S}^{\mathrm{c}}}$ denotes the optimal value of (AO) under the restriction of $\boldsymbol{w} \in \mathcal{S}^{\mathrm{c}}$. Hence, by setting $\bar{\phi} = \phi^*, \eta = \tilde{\eta}/3$ in Theorem II.1, we can use CGMT for $\mathcal{S}$, i.e., Lemma IV.1 holds not only for the optimizer $\hat{\boldsymbol{w}}_N$ of (AO) but also for that of (PO). We thus conclude the proof.

Remark IV.1. The optimal value α^* is related to the asymptotic MSE as is the case of [24]. In fact, from the definition of α_N^* and (69), $(\alpha_N^*)^2$ can be written as

$$(\alpha_N^*)^2 = \frac{\|\hat{\boldsymbol{w}}_N\|_2^2}{N} + \sigma_{\mathrm{v}}^2, \tag{79}$$

where $\hat{\boldsymbol{w}}_N$ is the optimal value of (AO). Given that $\alpha_N^* \xrightarrow{\mathrm{P}} \alpha^*$, we have

$$\hat{\boldsymbol{w}}_N \in \mathcal{S}_{\mathrm{MSE}} \coloneqq \left\{ \boldsymbol{z} \in \mathbb{R}^N \;\middle|\; \left| \frac{\|\boldsymbol{z}\|_2^2}{N} - (\alpha^*)^2 + \sigma_{\mathrm{v}}^2 \right| < \varepsilon \right\}, \tag{80}$$

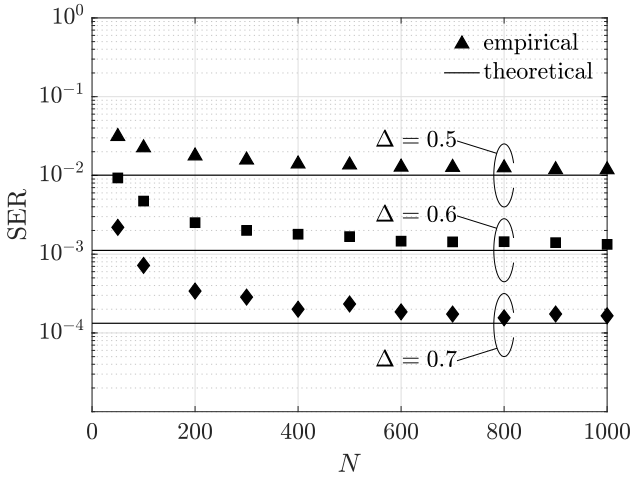

Fig. 11: SER of Box-SOAV versus N ($(r_1, r_2) = (0, 1)$, $(p_1, p_2) = (0.8, 0.2)$, SNR $= 15$ dB)

with probability approaching 1 as $N \to \infty$ for any ε (> 0). By using CGMT for $\mathcal{S}_{\mathrm{MSE}}$, we obtain $\hat{\boldsymbol{x}} - \boldsymbol{x} \in \mathcal{S}_{\mathrm{MSE}}$ with probability approaching 1, i.e.,

$$\operatorname*{plim}_{N\to\infty} \frac{1}{N}\|\hat{\boldsymbol{x}} - \boldsymbol{x}\|_2^2 = (\alpha^*)^2 - \sigma_{\mathrm{v}}^2. \tag{81}$$

V. Simulation Results

In this section, we compare the theoretical results by Corollary III.1 and the empirical performance obtained by computer simulations. In the simulations, the measurement matrix $\boldsymbol{A} \in \mathbb{R}^{M\times N}$ and the noise vector $\boldsymbol{v} \in \mathbb{R}^M$ satisfy the assumptions in Theorem III.1. For the calculation of α^* and β^*, we use the ternary search with the error tolerance $\varepsilon_{\mathrm{tol}} = 10^{-6}$.

We firstly compare the empirical performance of the Box-SOAV optimization with the theoretical result. Figure 11 shows the SER performance for the binary vector with $(r_1, r_2) = (0, 1)$ for measurement ratios of $\Delta = 0.5, 0.6$, and 0.7. The distribution of the unknown vector is given by $(p_1, p_2) = (0.8, 0.2)$. The SNR is 15 dB. We use $\mathcal{Q}_{\mathrm{AO}}(\cdot)$ as the quantizer and the parameter of Box-SOAV is optimized as in Example III.1. In the figure, 'empirical' represents the empirical performance obtained by averaging the SER over 2000 independent realizations of the measurement matrix. We use Douglas-Rachford algorithm [38], [40] to solve the Box-SOAV optimization problem. We can see that the theoretical prediction denoted by 'theoretical' agrees well with the empirical performance for large N.

Next, we show that the proposed optimal parameters and quantizer can achieve better performance than some fixed parameter and the naive quantizer. Figure 12 shows the SER performance of the Box-SOAV optimization versus the SNR, where $N = 1000$, $\Delta = 0.8$, $(r_1, r_2, r_3) = (-1, 0, 1)$, and $(p_1, p_2, p_3) = (0.1, 0.8, 0.1)$. As described in Example III.2, the parameter of the Box-SOAV optimization is only q_2 in this case. In the figure, '$q_2 = 0.01$' and '$q_2 = 0.1$' denote the performance of the Box-SOAV optimization with $q_2 = 0.01$ and $q_2 = 0.1$, respectively. We use the naive quantizer $\mathcal{Q}_{\mathrm{NV}}(\cdot)$ in (21) for these methods. Also, 'optimal' represents the

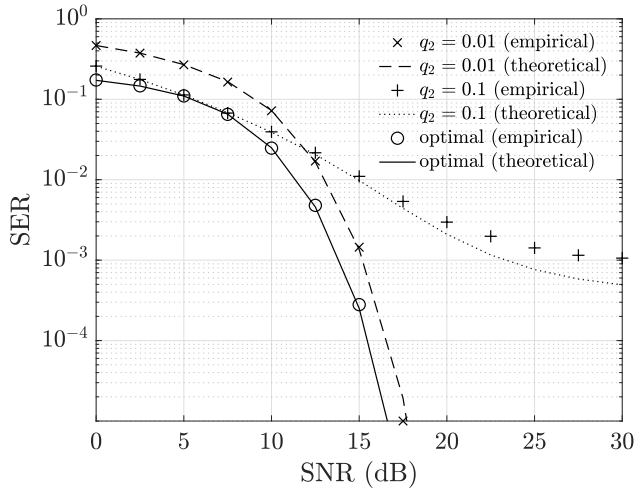

Fig. 12: SER of Box-SOAV versus the SNR ($N = 1000$, $\Delta = 0.8$, $(r_1, r_2, r_3) = (-1, 0, 1)$, $(p_1, p_2, p_3) = (0.1, 0.8, 0.1)$)

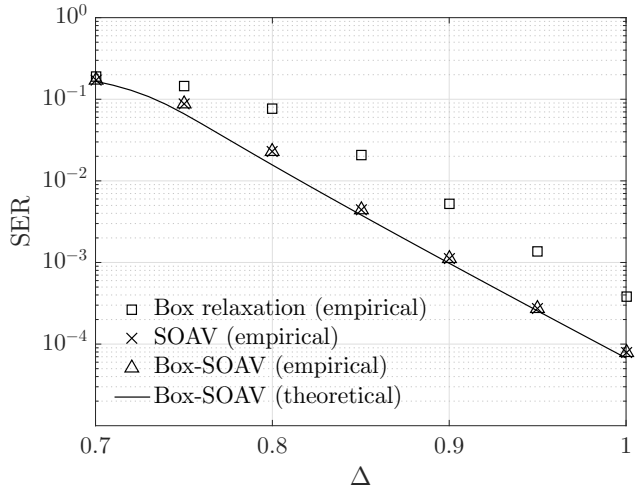

Fig. 13: SER versus $\Delta = M/N$ ($N = 1500$, $(r_1, r_2, r_3) = (-1, 0, 1)$, $(p_1, p_2, p_3) = (0.25, 0.5, 0.25)$, SNR $= 20$ dB)

performance of the Box-SOAV optimization with the proposed asymptotically optimal parameter and quantizer $\mathcal{Q}_{\mathrm{AO}}(\cdot)$. We can see that the proposed parameter and quantizer outperforms the fixed parameter and the naive quantizer. It should be noted that the optimal value of q_2 clearly depends on the SNR and the proposed approach can determine the asymptotically optimal value adaptively if the SNR is known in advance.

Finally, we compare the performance of the Box-SOAV optimization with some conventional methods. Figure 13 shows the SER performance versus Δ for the unknown discrete-valued vector with $(r_1, r_2, r_3) = (-1, 0, 1)$. We assume $N = 1500$, $(p_1, p_2, p_3) = (0.25, 0.5, 0.25)$, and the SNR of 20 dB. In the figure, 'SOAV' and 'Box-SOAV' represent the conventional SOAV optimization and the Box-SOAV optimization, respectively. We use $\mathcal{Q}_{\mathrm{AO}}(\cdot)$ as the quantizer and the parameter of Box-SOAV is optimized as in Example III.2. For comparison, we also evaluate the performance of the box relaxation method [9], [10] given by

$$\min_{\boldsymbol{s}\in[-1,1]^N} \frac{1}{2} \|\boldsymbol{y} - \boldsymbol{A}\boldsymbol{s}\|_2^2 . \tag{82}$$

From the figure, we can see that the empirical performances of Box-SOAV and SOAV are close to the theoretical prediction of Box-SOAV. Moreover, they have better performance than the box relaxation method because they effectively use the knowledge of the distribution of the unknown vector.

VI. Conclusion

In this paper, we have derived the theoretical asymptotic performance of the discrete-valued vector reconstruction using the Box-SOAV optimization, which is the combination of the conventional box relaxation method and the SOAV optimization. By using the CGMT framework, we have shown that the asymptotic SER can be obtained with Corollary III.1. Moreover, we have derived the asymptotic distribution of the estimate obtained by the Box-SOAV optimization. The empirical estimate of the Box-SOAV optimization is characterized by the random variable $\hat{X}$ in the large system limit. This means that the reconstruction process by the Box-SOAV optimization can be decoupled into the corresponding scalar system in the asymptotic regime. The asymptotic results enable us to obtain the optimal parameters of the Box-SOAV optimization and the asymptotically optimal quantizer. In Examples III.1–III.3, we have shown the derivation, the effectiveness, and the sensitivity of the quantizer for several instances of the reconstruction problem. Simulation results show that the empirical performance agrees well with the theoretical prediction of Corollary III.1 when the problem size is sufficiently large. We have also shown that we can improve the performance of the Box-SOAV optimization by using the proposed asymptotically optimal parameters and quantizer.

Future work includes the extension of the analysis to the reconstruction of the complex discrete-valued vector. The box relaxation method can be extended for the complex discrete-valued vector, and the theoretical performance has been analyzed in [34]. On the other hand, although the SOAV optimization has also been extended for the complex discrete-valued vector [50], the theoretical aspects has not been known sufficiently. The techniques in [34] might be useful to obtain the asymptotic performance of the method in [50]. As another research direction, it would be interesting to consider the unknown discrete-valued vector obtained by the quantization of a continuous-valued vector. It might be possible to optimize the initial quantization by our approach as in the rate-distortion theory [51].

Appendix A
Proof of Corollary III.1

Let $\psi(w, x) = 1 - \chi(w + x, x)$ in Theorem III.1, where the function $\chi(\cdot, \cdot) : [r_1, r_L] \times \mathcal{R} \to \{0, 1\}$ is given by

$$\chi(\hat{x}, x) = \begin{cases} 1 & (\mathcal{Q}(\hat{x}) = x) \\ 0 & (\mathcal{Q}(\hat{x}) \neq x) \end{cases} . \tag{83}$$

The left hand side of (16) can be written as

$$\operatorname*{plim}_{N\to\infty} \frac{1}{N} \sum_{n=1}^{N} (1 - \chi(\hat{x}_n, x_n)) = \operatorname*{plim}_{N\to\infty} \frac{1}{N} \|\mathcal{Q}(\hat{\boldsymbol{x}}) - \boldsymbol{x}\|_0 , \tag{84}$$

whereas the right hand side can be written as

$$\mathrm{E}\left[1-\chi(\hat{X},X)\right] = 1-\Pr\left(\mathcal{Q}(\hat{X})=X\right) \tag{85}$$

$$= 1-\sum_{\ell=1}^{L} p_\ell \Pr\left(\mathcal{Q}(\hat{X})=r_\ell \mid X=r_\ell\right), \tag{86}$$

which concludes (20). Although $\chi(\cdot, r_\ell)$ is not Lipschitz continuous, we can approximate $\chi(\cdot, r_\ell)$ with a Lipschitz function because H is a continuous random variable and the probability measure for the discontinuity point of $\chi(\cdot, r_\ell)$ is zero (For a similar discussion, see [23, Lemma A.4]).

Appendix B
Proof of Theorem III.2

It is sufficient to prove

$$\lim_{N\to\infty}\Pr\left(\left|\int g\,d\mu_{\hat{\boldsymbol{x}}} - \int g\,d\mu_{\hat{X}}\right| < \varepsilon\right) = 1 \tag{87}$$

for any $\varepsilon > 0$. From the Stone-Weierstrass theorem [52], there exists a polynomial $\nu(\cdot) : [r_1, r_L] \to \mathbb{R}$ such that

$$|g(x)-\nu(x)| < \frac{\varepsilon}{3} \tag{88}$$

for any $x \in [r_1, r_L]$. Hence, the absolute value in (87) can be upper bounded as

$$\left|\int g\,d\mu_{\hat{\boldsymbol{x}}} - \int g\,d\mu_{\hat{X}}\right|$$
$$\le \left|\int g\,d\mu_{\hat{\boldsymbol{x}}} - \int \nu\,d\mu_{\hat{\boldsymbol{x}}}\right| + \left|\int \nu\,d\mu_{\hat{\boldsymbol{x}}} - \int \nu\,d\mu_{\hat{X}}\right| + \left|\int \nu\,d\mu_{\hat{X}} - \int g\,d\mu_{\hat{X}}\right| \tag{89}$$

$$< \left|\int \nu\,d\mu_{\hat{\boldsymbol{x}}} - \int \nu\,d\mu_{\hat{X}}\right| + \frac{2}{3}\varepsilon \tag{90}$$

Note that the polynomial $\nu(\cdot)$ is Lipschitz in $[r_1, r_L]$. We then define $\psi(w,x) = \nu(w+x)$ in Theorem III.1 and obtain $\operatorname{plim}_{N\to\infty} \frac{1}{N}\sum_{n=1}^{N} \nu(\hat{x}_n) = \mathrm{E}\left[\nu(\hat{X})\right]$, i.e.,

$$\lim_{N\to\infty}\Pr\left(\left|\int \nu\,d\mu_{\hat{\boldsymbol{x}}} - \int \nu\,d\mu_{\hat{X}}\right| < \frac{\varepsilon}{3}\right) = 1. \tag{91}$$

(90) and (91) conclude (87).

Appendix C
Proof of Lemma IV.1

Let $\theta(h_n, x_n) = \operatorname{prox}_{\frac{\alpha^*}{\beta^*\sqrt{\Delta}} f}\left(x_n + \frac{\alpha^*}{\sqrt{\Delta}} h_n\right) - x_n$. From the law of large numbers, we have

$$\operatorname*{plim}_{N\to\infty} \frac{1}{N}\sum_{n=1}^{N} \psi(\theta(h_n, x_n), x_n) = \mathrm{E}\left[\psi\left(\hat{X}-X, X\right)\right]. \tag{92}$$

Hence, it is sufficient to show

$$\operatorname*{plim}_{N\to\infty}\left|\frac{1}{N}\sum_{n=1}^{N}\left\{\psi(\hat{w}_{N,n}(h_n,x_n),x_n) - \psi(\theta(h_n,x_n),x_n)\right\}\right| = 0, \tag{93}$$

which is equivalent to

$$\lim_{N\to\infty}\Pr\left(\left|\frac{1}{N}\sum_{n=1}^{N}\left\{\psi(\hat{w}_{N,n}(h_n,x_n),x_n) - \psi(\theta(h_n,x_n),x_n)\right\}\right| < \varepsilon\right)$$
$$= \sum_{\ell=1}^{L} p_\ell \lim_{N\to\infty}\Pr\left(\left|\frac{1}{N}\sum_{n=1}^{N}\left\{\psi(\hat{w}_{N,n}(h_n,r_\ell),r_\ell) - \psi(\theta(h_n,r_\ell),r_\ell)\right\}\right| < \varepsilon\right) \tag{94}$$

$$= 1 \tag{95}$$

for any ε (> 0). We thus prove

$$\lim_{N\to\infty}\Pr\left(\left|\frac{1}{N}\sum_{n=1}^{N}\left\{\psi(\hat{w}_{N,n}(h_n,r_\ell),r_\ell) - \psi(\theta(h_n,r_\ell),r_\ell)\right\}\right| < \varepsilon\right) = 1 \tag{96}$$

for $\ell = 1, \ldots, L$ below.

If we denote the Lipschitz constant of $\psi(\cdot, r_\ell)$ by $C_{\psi,\ell}$, we have

$$|\psi(\hat{w}_{N,n}(h_n,r_\ell),r_\ell) - \psi(\theta(h_n,r_\ell),r_\ell)| \le C_{\psi,\ell}\,|\hat{w}_{N,n}(h_n,r_\ell) - \theta(h_n,r_\ell)|. \tag{97}$$

The absolute value in the right hand side of (97) is upper bounded as

$$|\hat{w}_{N,n}(h_n,r_\ell) - \theta(h_n,r_\ell)|$$
$$\le \left|\operatorname{prox}_{\frac{\alpha_N^*}{\beta_N^*}\frac{\sqrt{N}}{\|\boldsymbol{g}\|_2} f}\left(r_\ell + \frac{\sqrt{N}}{\|\boldsymbol{g}\|_2}\alpha_N^* h_n\right) - \operatorname{prox}_{\frac{\alpha_N^*}{\beta_N^*}\frac{\sqrt{N}}{\|\boldsymbol{g}\|_2} f}\left(r_\ell + \frac{\alpha^*}{\sqrt{\Delta}} h_n\right)\right|$$
$$+ \left|\operatorname{prox}_{\frac{\alpha_N^*}{\beta_N^*}\frac{\sqrt{N}}{\|\boldsymbol{g}\|_2} f}\left(r_\ell + \frac{\alpha^*}{\sqrt{\Delta}} h_n\right) - \operatorname{prox}_{\frac{\alpha^*}{\beta^*\sqrt{\Delta}} f}\left(r_\ell + \frac{\alpha^*}{\sqrt{\Delta}} h_n\right)\right| \tag{98}$$

$$\le \left|\frac{\sqrt{N}}{\|\boldsymbol{g}\|_2}\alpha_N^* h_n - \frac{\alpha^*}{\sqrt{\Delta}} h_n\right|$$
$$+ \left|\operatorname{prox}_{\frac{\alpha_N^*}{\beta_N^*}\frac{\sqrt{N}}{\|\boldsymbol{g}\|_2} f}\left(r_\ell + \frac{\alpha^*}{\sqrt{\Delta}} h_n\right) - \operatorname{prox}_{\frac{\alpha^*}{\beta^*\sqrt{\Delta}} f}\left(r_\ell + \frac{\alpha^*}{\sqrt{\Delta}} h_n\right)\right|. \tag{99}$$

In (99), we use the fact that $\operatorname{prox}_{\gamma f}(\cdot)$ is non-expansive. For the first term in (99), we have $\left|\frac{\sqrt{N}}{\|\boldsymbol{g}\|_2}\alpha_N^* h_n - \frac{\alpha^*}{\sqrt{\Delta}} h_n\right| \xrightarrow{\mathrm{P}} 0$ as

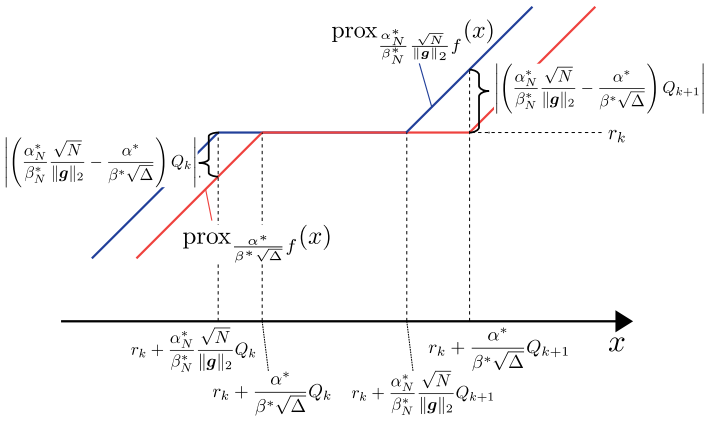

Fig. 14: Graphical representation for (100).

$N\to\infty$. Moreover, given that $\frac{\alpha_N^*}{\beta_N^*}\frac{\sqrt{N}}{\|\boldsymbol{g}\|_2}$ is sufficiently close to $\frac{\alpha^*}{\beta^*\sqrt{\Delta}}$ when N is large, the second term is upper bounded as

$$\left|\mathrm{prox}_{\frac{\alpha_N^*}{\beta_N^*}\frac{\sqrt{N}}{\|\boldsymbol{g}\|_2}f}\left(r_\ell+\frac{\alpha^*}{\sqrt{\Delta}}h_n\right)-\mathrm{prox}_{\frac{\alpha^*}{\beta^*\sqrt{\Delta}}f}\left(r_\ell+\frac{\alpha^*}{\sqrt{\Delta}}h_n\right)\right|$$

$$\le\max_{k=2,\ldots,L}\left\{\left|\left(\frac{\alpha_N^*}{\beta_N^*}\frac{\sqrt{N}}{\|\boldsymbol{g}\|_2}-\frac{\alpha^*}{\beta^*\sqrt{\Delta}}\right)Q_k\right|\right\} \tag{100}$$

$$\xrightarrow{\mathrm{P}}0 \tag{101}$$

as $N\to\infty$ (See Fig. 14). We thus have $|\psi(\hat{w}_n(h_n,r_\ell),r_\ell)-\psi(\theta(h_n,r_\ell),r_\ell)|\xrightarrow{\mathrm{P}}0$ and obtain (96), which completes the proof.

REFERENCES

[1] A. Chockalingam and B. S. Rajan, *Large MIMO Systems*. Cambridge, U.K.: Cambridge University Press, 2014.
[2] S. Yang and L. Hanzo, "Fifty years of MIMO detection: The road to large-scale MIMOs," *IEEE Commun. Surv. Tutor.*, vol. 17, no. 4, pp. 1941–1988, Fourthquarter 2015.
[3] S. Verdú, *Multiuser Detection*, 1st ed. New York, NY, USA: Cambridge University Press, 1998.
[4] S. K. Mohammed, A. Zaki, A. Chockalingam, and B. S. Rajan, "High-rate space–time coded large-MIMO systems: Low-complexity detection and channel estimation," *IEEE J. Sel. Top. Signal Process.*, vol. 3, no. 6, pp. 958–974, Dec. 2009.
[5] K. K. Wong, A. Paulraj, and R. D. Murch, "Efficient high-performance decoding for overloaded MIMO antenna systems," *IEEE Trans. Wirel. Commun.*, vol. 6, no. 5, pp. 1833–1843, May 2007.
[6] T. Takahashi, S. Ibi, and S. Sampei, "Criterion of adaptively scaled belief for PDA in overloaded MIMO channels," in *Proc. 51st Asilomar Conference on Signals, Systems, and Computers*, Oct. 2017, pp. 1094–1098.
[7] S. Takabe, M. Imanishi, T. Wadayama, R. Hayakawa, and K. Hayashi, "Trainable projected gradient detector for massive overloaded MIMO channels: Data-driven tuning approach," *IEEE Access*, vol. 7, pp. 93 326–93 338, 2019.
[8] J. B. Anderson, F. Rusek, and V. Öwall, "Faster-than-Nyquist signaling," *Proc. IEEE*, vol. 101, no. 8, pp. 1817–1830, Aug. 2013.
[9] P. H. Tan, L. K. Rasmussen, and T. J. Lim, "Constrained maximum-likelihood detection in CDMA," *IEEE Trans. Commun.*, vol. 49, no. 1, pp. 142–153, Jan. 2001.
[10] A. Yener, R. D. Yates, and S. Ulukus, "CDMA multiuser detection: A nonlinear programming approach," *IEEE Trans. Commun.*, vol. 50, no. 6, pp. 1016–1024, Jun. 2002.
[11] A. Aïssa-El-Bey, D. Pastor, S. M. A. Sbaï, and Y. Fadlallah, "Sparsity-based recovery of finite alphabet solutions to underdetermined linear systems," *IEEE Trans. Inf. Theory*, vol. 61, no. 4, pp. 2008–2018, Apr. 2015.
[12] D. L. Donoho, "Compressed sensing," *IEEE Trans. Inf. Theory*, vol. 52, no. 4, pp. 1289–1306, Apr. 2006.
[13] K. Hayashi, M. Nagahara, and T. Tanaka, "A user's guide to compressed sensing for communications systems," *IEICE Trans. Commun.*, vol. E96-B, no. 3, pp. 685–712, Mar. 2013.
[14] M. Nagahara, "Discrete signal reconstruction by sum of absolute values," *IEEE Signal Process. Lett.*, vol. 22, no. 10, pp. 1575–1579, Oct. 2015.
[15] H. Sasahara, K. Hayashi, and M. Nagahara, "Symbol detection for faster-than-Nyquist signaling by sum-of-absolute-values optimization," *IEEE Signal Process. Lett.*, vol. 23, no. 12, pp. 1853–1857, Dec. 2016.
[16] T. Ikeda, M. Nagahara, and S. Ono, "Discrete-valued control of linear time-invariant systems by sum-of-absolute-values optimization," *IEEE Trans. Autom. Control*, vol. 62, no. 6, pp. 2750–2763, Jun. 2017.
[17] H. Sasahara, K. Hayashi, and M. Nagahara, "Multiuser detection based on MAP estimation with sum-of-absolute-values relaxation," *IEEE Trans. Signal Process.*, vol. 65, no. 21, pp. 5621–5634, Nov. 2017.
[18] R. Hayakawa and K. Hayashi, "Error recovery for massive MIMO signal detection via reconstruction of discrete-valued sparse vector," *IEICE Trans. Fundam. Electron. Commun. Comput. Sci.*, vol. E100-A, no. 12, pp. 2671–2679, Dec. 2017.
[19] ——, "Convex optimization-based signal detection for massive overloaded MIMO systems," *IEEE Trans. Wirel. Commun.*, vol. 16, no. 11, pp. 7080–7091, Nov. 2017.
[20] T. Ikeda and M. Nagahara, "Discrete-valued model predictive control using sum-of-absolute-values optimization," *Asian J. Control*, vol. 20, no. 1, pp. 196–206, 2018.
[21] R. Hayakawa and K. Hayashi, "Discreteness-aware decoding for overloaded non-orthogonal STBCs via convex optimization," *IEEE Commun. Lett.*, vol. 22, no. 10, pp. 2080–2083, Oct. 2018.
[22] K. Hayashi, A. Nakai, R. Hayakawa, and S. Ha, "Uplink overloaded MU-MIMO OFDM signal detection methods using convex optimization," in *Proc. Asia-Pacific Signal and Information Processing Association Annual Summit and Conference (APSIPA ASC)*, Nov. 2018, pp. 1421–1427.
[23] C. Thrampoulidis, W. Xu, and B. Hassibi, "Symbol error rate performance of box-relaxation decoders in massive MIMO," *IEEE Trans. Signal Process.*, vol. 66, no. 13, pp. 3377–3392, Jul. 2018.
[24] C. Thrampoulidis, E. Abbasi, and B. Hassibi, "Precise error analysis of regularized M-estimators in high dimensions," *IEEE Trans. Inf. Theory*, vol. 64, no. 8, pp. 5592–5628, Aug. 2018.
[25] C. Thrampoulidis, A. Panahi, D. Guo, and B. Hassibi, "Precise error analysis of the LASSO," in *Proc. IEEE International Conference on Acoustics, Speech and Signal Processing (ICASSP)*, Apr. 2015, pp. 3467–3471.
[26] C. Thrampoulidis, A. Panahi, and B. Hassibi, "Asymptotically exact error analysis for the generalized ℓ_2^2-LASSO," in *Proc. IEEE International Symposium on Information Theory (ISIT)*, Jun. 2015, pp. 2021–2025.
[27] C. Thrampoulidis, S. Oymak, and B. Hassibi, "Regularized linear regression: A precise analysis of the estimation error," in *Proc. Conference on Learning Theory*, Jun. 2015, pp. 1683–1709.
[28] I. B. Atitallah, C. Thrampoulidis, A. Kammoun, T. Y. Al-Naffouri, M. Alouini, and B. Hassibi, "The BOX-LASSO with application to GSSK modulation in massive MIMO systems," in *Proc. IEEE International Symposium on Information Theory (ISIT)*, Jun. 2017, pp. 1082–1086.
[29] C. Thrampoulidis, E. Abbasi, W. Xu, and B. Hassibi, "BER analysis of the box relaxation for BPSK signal recovery," in *Proc. IEEE International Conference on Acoustics, Speech and Signal Processing (ICASSP)*, Mar. 2016, pp. 3776–3780.
[30] C. Thrampoulidis, E. Abbasi, and B. Hassibi, "LASSO with non-linear measurements is equivalent to one with linear measurements," in *Proc. the 28th International Conference on Neural Information Processing Systems - Volume 2*, ser. NIPS'15. Montreal, Canada: MIT Press, 2015, pp. 3420–3428.
[31] C. Thrampoulidis and W. Xu, "The performance of box-relaxation decoding in massive MIMO with low-resolution ADCs," in *Proc. IEEE Statistical Signal Processing Workshop (SSP)*, Jun. 2018, pp. 821–825.
[32] A. M. Alrashdi, I. B. Atitallah, T. Y. Al-Naffouri, and M. Alouini, "Precise performance analysis of the LASSO under matrix uncertainties," in *Proc. IEEE Global Conference on Signal and Information Processing (GlobalSIP)*, Nov. 2017, pp. 1290–1294.
[33] A. M. Alrashdi, I. B. Atitallah, T. Ballal, C. Thrampoulidis, A. Chaaban, and T. Y. Al-Naffouri, "Optimum training for MIMO BPSK transmission," in *Proc. IEEE 19th International Workshop on Signal Processing Advances in Wireless Communications (SPAWC)*, Jun. 2018, pp. 1–5.
[34] E. Abbasi, F. Salehi, and B. Hassibi, "Performance analysis of convex data detection in MIMO," in *Proc. IEEE International Conference on*

Acoustics, Speech and Signal Processing (ICASSP), May 2019, pp. 4554–4558.
[35] R. Hayakawa and K. Hayashi, "Performance analysis of discrete-valued vector reconstruction based on box-constrained sum of L1 regularizers," in *Proc. IEEE International Conference on Acoustics, Speech and Signal Processing (ICASSP)*, May 2019, pp. 4913–4917.
[36] Y. Fadlallah, A. Aïssa-El-Bey, K. Amis, D. Pastor, and R. Pyndiah, "New iterative detector of MIMO transmission using sparse decomposition," *IEEE Trans. Veh. Technol.*, vol. 64, no. 8, pp. 3458–3464, Aug. 2015.
[37] Z. Hajji, A. Aïssa-El-Bey, and K. Amis, "Simplicity-based recovery of finite-alphabet signals for large-scale MIMO systems," *Digital Signal Processing*, vol. 80, pp. 70–82, Sep. 2018.
[38] P. L. Combettes and J.-C. Pesquet, "Proximal splitting methods in signal processing," in *Fixed-Point Algorithms for Inverse Problems in Science and Engineering*, ser. Springer Optimization and Its Applications. New York, NY: Springer New York, 2011, vol. 49, pp. 185–212.
[39] A. Beck and M. Teboulle, "A fast iterative shrinkage-thresholding algorithm for linear inverse problems," *SIAM J. Imaging Sci.*, vol. 2, no. 1, pp. 183–202, Jan. 2009.
[40] P. Lions and B. Mercier, "Splitting algorithms for the sum of two nonlinear operators," *SIAM J. Numer. Anal.*, vol. 16, no. 6, pp. 964–979, Dec. 1979.
[41] J. Eckstein and D. P. Bertsekas, "On the Douglas-Rachford splitting method and the proximal point algorithm for maximal monotone operators," *Mathematical Programming*, vol. 55, no. 1, pp. 293–318, Apr. 1992.
[42] E. J. Candès, "The restricted isometry property and its implications for compressed sensing," *Comptes Rendus Mathematique*, vol. 346, no. 9, pp. 589–592, May 2008.
[43] R. Tibshirani, "Regression Shrinkage and Selection via the Lasso," *J. R. Stat. Soc. Ser. B Methodol.*, vol. 58, no. 1, pp. 267–288, 1996.
[44] D. L. Donoho, A. Maleki, and A. Montanari, "Message-passing algorithms for compressed sensing," *PNAS*, vol. 106, no. 45, pp. 18 914–18 919, Nov. 2009.
[45] S. Rangan, "Generalized approximate message passing for estimation with random linear mixing," in *Proc. IEEE International Symposium on Information Theory (ISIT)*, Jul. 2011, pp. 2168–2172.
[46] C. Jeon, R. Ghods, A. Maleki, and C. Studer, "Optimality of large MIMO detection via approximate message passing," in *Proc. IEEE International Symposium on Information Theory (ISIT)*, Jun. 2015, pp. 1227–1231.
[47] D. G. Luenberger and Y. Ye, "Basic Descent Methods," in *Linear and Nonlinear Programming*, ser. International Series in Operations Research & Management Science. New York, NY: Springer US, 2008, pp. 215–262.
[48] M. A. Suliman, A. M. Alrashdi, T. Ballal, and T. Y. Al-Naffouri, "SNR estimation in linear systems with Gaussian matrices," *IEEE Signal Process. Lett.*, vol. 24, no. 12, pp. 1867–1871, Dec. 2017.
[49] R. Hayakawa and K. Hayashi, "Discreteness-aware approximate message passing for discrete-valued vector reconstruction," *IEEE Trans. Signal Process.*, vol. 66, no. 24, pp. 6443–6457, Dec. 2018.
[50] ——, "Reconstruction of complex discrete-valued vector via convex optimization with sparse regularizers," *IEEE Access*, vol. 6, pp. 66 499–66 512, 2018.
[51] T. M. Cover and J. A. Thomas, *Elements of Information Theory (Wiley Series in Telecommunications and Signal Processing)*. USA: Wiley-Interscience, 2006.
[52] D. Pérez and Y. Quintana, "A survey on the Weierstrass approximation theorem," *Divulg. Matemáticas*, vol. 16, no. 1, pp. 231–247, 2008.

PLACE PHOTO HERE

Ryo Hayakawa received the bachelor's degree in engineering, the master's degree in informatics, and Ph.D. degree in informatics from Kyoto University, Kyoto, Japan, in 2015, 2017, and 2020, respectively. He is currently an Assistant Professor at Graduate School of Engineering Science, Osaka University. He was a Research Fellow (DC1) of the Japan Society for the Promotion of Science (JSPS) from 2017 to 2020. He received the 33rd Telecom System Technology Student Award, APSIPA ASC 2019 Best Special Session Paper Nomination Award, and the 16th IEEE Kansai Section Student Paper Award. His research interests include signal processing and wireless communication. He is a member of IEICE.

PLACE PHOTO HERE

Kazunori Hayashi is currently a Professor at Center for Innovative Research and Education in Data Science / Graduate School of Informatics, Kyoto University. He received the B.E., M.E., and Ph.D. degrees in communication engineering from Osaka University, Osaka, Japan, in 1997, 1999 and 2002, respectively. He was an Assistant Professor from 2002 to 2007, an Associate Professor from 2007 to 2017 at Graduate School of Informatics, Kyoto University, and a Professor from 2017 to 2020 at Graduate School of Engineering, Osaka City University. His research interests include statistical signal processing for communication systems. He received the ICF Research Award from the KDDI Foundation in 2008, the IEEE Globecom 2009 Best Paper Award, the IEICE Communications Society Best Paper Award in 2010, the WPMC'11 Best Paper Award, the Telecommunications Advancement Foundation Award in 2012, and the IEICE Communications Society Best Tutorial Paper Award in 2013. He is a member of IEICE, APSIPA, and ISCIE.